Chemical composition of giant planet hosts

Frida Ekstrand

Lund Observatory
Lund University

2017-EXA123

Degree project of 15 higher education credits
May 2017

Supervisor: Fan Liu

Lund Observatory
Box 43
SE-221 00 Lund
Sweden

Abstract

Does the formation of planets give imprints on the chemical composition of the host star? In order to test this theory a differential abundance analysis (i.e. comparing two stars' abundances to each other) was carried out on a few stars with and without known planets, to see if any differences were found. The analysis was based on high resolution, high signal to noise ratio (SNR) spectra of four stars: HD 102117, HD 90722, HIP 79672 (18 Sco) and the Sun, where two of the stars host known planets (Sun and HD 102117). Between two solar spectra, observed with two different instruments, no systematic offset was identified, and thus my result does not rely on the choice of the different spectrographs. A comparison between HIP 79672 and the Sun was performed and our results agree well with that from previous literature. When HD 102117 was compared to its stellar twin in the sample, HD 90722, I found that HD 102117 is more metal-poor by 0.05 dex. This difference could possibly be due to the formation of its gas giant. As a rough estimate, adding 7-9 $M_{\oplus}$ of an equal mixture of earth-like material and meteorite material to the convective zone of HD 102117 would even out the difference in average refractory abundance, in comparison to HD 90722. A trend with condensation temperature (T_c, the temperature at which an element condensate) was found as well. Since the mass of the planet's core is small, the imprinted T_c trend is not very clear, but could be improved with higher precision.

Populärvetenskaplig beskrivning

De stjärnor man kan se på himmeln en riktigt stjärnklar natt - omkring 3000 - är bara en bråkdel av alla de som faktiskt finns i universum. Ljuset har en hög men inte oändlig hastighet. Därför kan vi bara se sådant som ligger tillräckligt nära jorden, så att ljuset hunnit färdas hit under universums livstid. De himlakroppar som ligger längst bort ifrån jorden men som fortfarande går att se (med teleskop), ligger på ett avstånd av hisnande 93 miljarder ljusår! Alla dessa stjärnor skiner, precis som solen, men vissa skillnader i ljuset kan utrönas om man undersöker det närmre.

Hur ljuset ser ut beror på vilka ämnen stjärnan består av. Järn, till exempel skickar ut ljus med olika distinkta våglängder som går att urskilja från annat ljus. Om dessa våglängder syns i stjärnans spektrum (det mätta ljuset från stjärnan) kan man därför fastställa att den innehåller just järn och även hur mycket det finns. Alla ämnen som finns i stjärnan bidrar därför till ett specifikt fingeravtryck som kan användas för att undersöka stjärnors egenskaper, fastän de ligger så långt bort.

Solens egenskaper och uppbyggnad har gått att bestämma väldigt noggrant. Även hur mycket det finns av olika ämnen i de yttersta skikten har identifierats, det vill säga deras fingeravtryck har bestämts. Detsamma har gjorts med "sol-tvillingar", stjärnor som liknar solen i exempelvis temperatur och storlek, som inte har några planeter. När dessa har jämförts med solen har man hittat vissa tydliga skillnader som tyder på att solen saknar en del av de ämnen som man vanligtvis hittar i andra himlakroppar, så som stenplaneter (jordlika) och asteroider. Det skulle kunna betyda att solsystemets planeter har tagit ämnen som annars skulle ha funnits i solen, vilket gör att en skillnad i jämförelse med sol-tvillingarna (utan planeter) syns.

I början av solens liv fanns en disk runt den, bestående av gas och stoft. I denna disk bildades så småningom solsystemets planeter. När planeterna hade formats klart och resten av diskens stoft och gas hade samlats upp/blivit en del av solen, fattades en del planetämnen som kunde bidra till solens slutliga sammansättning.

Forskare försöker hitta fler sådana samband mellan planeter och vilka ämnen dess stjärna består av för att bättre förstå hur, och under vilka omständigheter, planeter formas. Vårt solsystem är relativt unikt med sina inre stenplaneter och yttre gasjättar. Till skillnad från vårt solsystem finns det många system som har en stor gasplanet i en väldigt nära omloppsbana runt stjärnan. I detta projekt undersöks om det finns någon skillnad i stjärnsammansättningen beroende på om stjärnan har en gasjätte i en nära eller avlägsen omloppsbana, alltså om stjärnans fingeravtryck ändras beroende på vilket avstånd dess planet finns.

Trots att alla stjärnor som vi kan se ligger så otroligt långt bort vet vi förvånansvärt mycket om dem. Till exempel hur stora de är, hur gamla, vilka ämnen de består av och hur mycket av ämnena det finns. Att det går att ta reda på så mycket, bara genom att titta på ljuset som kommer till oss, är nog inget de flesta tänker på när de blickar upp mot himlen en molnfri natt.

Contents

List of Figures

List of Tables

Chapter 1

Introduction

In recent years, the method for stellar abundance determination has been developed enormously. With the developed technique, namely line-by-line differential chemical abundance analysis, the errors have subsided to unprecedented precision of two percent, a five-fold improvement over traditional analyses (Melendez et al. 2009). This technique makes it possible to detect small anomalies in the chemical composition of planet hosts, which could be due to planet formation.

Many stars, with different planetary systems and chemical composition, have been studied. Specific chemical signatures have been identified for various groups of planets, giving deeper understanding about how planet formation possibly affects the host star. Since it is easier to examine stars than planets, these signatures could be of help in finding exoplanets as well. In this Bachelor's project, the chemical composition of giant planet hosts were investigated to examine if there is any difference in chemical abundances between stars hosting either hot (close to host star) or cold (further away from host star) Jupiters.

Gonzalez (1997) studied the stellar metallicity - giant planet connection and found that stars hosting giant planets are more metal-rich. A possible scenario is that planetesimals form more efficiently around metal-rich stars. This relation was explored by Fischer & Valenti (2005), where they concluded that the relation only holds for giant planets. The result of Buchhave et al. (2012) supported this by saying that gas giants form more often around hosts with higher metallicity, but the correlation decreases for smaller gas planets and vanishes for terrestrial planets. Terrestrial planets were detected around stars of various metallicities. On the contrary, Wang & Fischer (2014) found planet-metallicity correlations for all kinds of planets, although much more prominent for gas giants. Therefore a clear stellar metallicity - planet relation had been identified for giant planets, while the correlation for smaller planets remains unclear. All planets occur more frequently around metal-rich stars, even though the factor for gas giants is much higher than for the other kinds. Gas giants occur $\approx$9.3 times more often around metal-rich stars than metal-poor and the factors for the gas dwarfs and terrestrials are $\approx$2 and $\approx$1.7, respectively.

The most thoroughly studied star yet is the one closest to us, the Sun. Melendez et al.

(2009) compared the Sun's chemical composition to solar twins and solar analogues (i.e., stars with identical/similar atmospheric parameters as the Sun). They found that in comparison to the majority of solar twins without known planets, the Sun shows a 20% depletion of refractory elements (elements with high condensation temperature, T_C, that is the temperature at which an element condensates) relative to volatiles (elements with low T_C). When comparing the Sun to solar analogues hosting giant planets, a similar chemical pattern was found as for the sun compared to solar twins without known planets. These observations suggest a solar composition that depends on elemental condensation temperature. A few different reasons for this pattern are discussed in Melendez et al. (2009)'s paper, but their conclusion is that it is possibly due to the formation of terrestrial planets, while the effect of giant planets is more unclear. Melendez et al. (2009) proposed the following hypothesis for the peculiar solar chemical composition: in the solar nebula, refractories form dust and grains. During the accretion epoch, these materials form rocks and planetesimals, keeping them from being accreted onto the Sun. However, if this was to give a noticeable effect, the accretion of depleted gas has to have happened when the Sun's convective zone had become thin. Since the analogues with giant planets do not show the same abundance pattern as the Sun, this suggests that the Sun's pattern is due to the inner terrestrial planets.

In Chambers (2010), it is suggested that the depletion in the Sun, relative to its twins, could be equated by adding 4 Earth-masses ($M_\oplus$) of rocky material to the convection zone. The convective zone is a region in the star where heat is transferred by the bulk motion of material, called convection. This would correspond to material that was not accreted, since it was held up in other objects. Various compositions of the rocky material were tested, but the one to conform best was equal amounts of Earth-like material and typical meteorite material. It has been thought that the convection zone usually remains large for a longer time than the gas disc's lifetime, but some models (Wuchterl & Tscharnuter 2003; Baraffe et al. 2009; Baraffe & Chabrier 2010) suggest that this may not be the case for solar-type stars. It suggests that the convection zone of the Sun, at the time when the gas was accreted, could have been of a similar size as it is today. The terrestrial planets' mass is collectively 2 $M_\oplus$, and the asteroid belt could earlier have contained about 2 earth-masses of proto-planets that were later ejected by Jupiter. Together, this could explain the difference between chemical abundances in the Sun and its twins. After adding this material, the Sun's abundance pattern fits well with the mean abundances of other studied solar twins in Chambers (2010). That the mixed material seems to be the best match infers that the Sun could potentially accreted material from both these regions.

Dissimilarities in abundance patterns are not only seen between single stars, but also in binary systems such as 16 Cygni (Tucci Maia et al. 2014), XO-2 (Ramírez et al. 2015), HD 133131 (Teske et al. 2016b) and WASP-94 (Teske et al. 2016a). In 16 Cygni, one of the stars is host to a gas giant with a minimum mass of 1.5 M_J (Jupiter-mass). It has been observed that the planet host is depleted in all elements, and a T_c-trend is identified when compared to the planetless companion (Tucci Maia et al. 2014). XO-2, as studied in Ramírez et al. (2015) contains two very similar stars, separated by 4500 au, and a total of 3 planets (two orbiting XO-2S and one around XO-2N). The planets' masses are > 0.26 M_J

and > 1.4 M_J respectively for 2S and > 0.6 M_J for 2N. By performing an high precision abundance analysis, it was determined that 2N is more metal-rich than 2S. Volatiles are about 3.5% more abundant while refractory elements are increased by approximately 23%. Thus, a clear T_C-trend is noticeable, as in the Sun. Assuming that the binary was formed from the same nebulae, and each star had its own planetary disc, the stars should have had the same chemical composition from the beginning. The difference in metallicity have thus presumably arisen during or after planet formation. From previously discussed research, it is known that a prominent T_C-trend could be the chemical signature imprinted by formation of terrestrial planets. Hence the deficiency of refractory elements in XO-2S could be present as a result of formation, or accretion, of yet non-detected rocky objects. The mass of these objects was assessed by the same method as in Chambers (2010), and yielded 20 $M_\oplus$ of rocky material to even out the difference. To explain the T_C-trend, 20 $M_\oplus$ more of rocky objects should have formed around 2S than 2N, or the same amount should have been accreted onto 2N. No terrestrial planets have yet been found around the stars. One suggestion is that the large planet around 2N has migrated into its present position and in that way dragged in large terrestrial planets to its host star.

Also a terrestrial-planet hosting star, Kepler-10, has been investigated (Liu et al. 2016b). Its planets have been characterised as an Earth-like planet with a mass of 3.33 $M_\oplus$ and a Neptune-like planet with mass of 17.3 $M_\oplus$. If the hypothesis about terrestrial planets causing depletion of refractories is true, this would show when comparing Kepler-10 to other similar stars without planets. The result obtained was in fact that Kepler-10, on average, showed a depletion in refractory elements relative to volatile, but that it differed depending on which comparison-star was used. For most of its stellar twins, the positive T_C-trend was evident, favouring the hypothesis proposed by Melendez et al. (2009). For two stellar twins there were no trend. This could mean that these comparison-stars host terrestrial planets that have not yet been discovered. The abundance difference corresponds to about 13 $M_\oplus$ of rocky material, which is comparable to the total mass of the known planets. Consequentially, the abundance pattern of Kepler-10 could possibly come from the formation of its planets, which supports the hypothesis of Melendez et al. (2009).

There are many possible explanations as to why there are anomalies in chemical abundances between stellar twins and the Sun. One hypothesis is planet formation where terrestrial planets give a T_C-trend in the abundance pattern, for example the XO-2 binary in Ramírez et al. (2015), while gas planets yield an overall offset in metallicity, e.g. the binary 16 Cygni in Ramírez et al. (2011). In Ramírez et al. (2015) the "north" component of the XO-2 binary is found to have a metal depletion with a clear T_c-trend possibly caused by the formation of rocky material. These signatures are not only established in the Sun, but also in other types of stars, which confirms the hypothesis. The calculated mass of rocky material needed to even out the differences conform well with the mass of the observed planets, which further supports the hypothesis. The possible chemical signatures of planet formation can help us to better understand the processes and circumstances involved in planet formation. Since terrestrial planets are relatively small, the differences in elemental abundances of the star are not extensive. In order to observe them, the convection zone at the time of gas accretion must have been close to

the present size. This could be used to understand the time scale of the formation of the planets.

As discussed before, gas giants give an overall offset in metallicity, but the migration of such large planets to smaller orbits may have other effects as well. In order to test this theory, a high precision differential abundance analysis is carried out on two sets of similar stars. The first: HD 102117 and HD 90722, and the second: the Sun and a solar twin, HIP 79672. For the Sun, two spectra are used, one reflected off the asteroid Juno and one off Hebe. In these two sets, HD 102117 (Tinney et al. 2005) and the Sun are the stars hosting giant planets. The planet around HD 102117 has a minimum mass of 0.17 M_J and orbits at a distance of about 0.15 au while Jupiter's orbit around the Sun has an approximate radius of 5 au. No planets have been found around HIP 79672 and HD 90722. Assuming the hypothesis that planet formation can imprint chemical signatures onto the host star, comparing the chemical composition of planet hosts to the similar stars without planets might yield abundance differences. Further, the two planet hosts are compared to see if the orbital distance of giant planets has any effect on the chemical composition of the host star. Up until now, mostly traditional techniques have been used to investigate how gas giants affect the abundances, but here a differential approach is used instead, yielding a higher precision.

Chapter 2

Method

2.1 Spectral line formation and chemical abundance analysis

Spectral lines of a star originate in the stellar photosphere (Gray 2005). Radiation is created by nuclear processes in the core and is then scattered outwards, performing a "random walk", until it reaches the photosphere. In the photosphere it keeps scattering until it reaches the point where the optical depth, τ_ν, is one. This is where the radiation can escape the star so we can observe it. The optical depth is the sum of the absorption coefficients, α_ν, from different absorption/scattering processes in a small distance dx in the star. Both the absorption coefficient and optical depth are frequency dependent and will thus be different for various wavelengths. The inverse of α_ν gives a measure of how far a photon can travel before being removed from the beam, i.e. the photon mean free path. At all frequencies, the light we see comes from an optical depth of $\tau_\nu = 1$ in the star. But since α_ν changes, the optical depth can be converted to geometrical depth by $1/\alpha_\nu$, allowing us to calculate at which depth in the star the light has originated from.

The source function, S_ν, is a ratio between emissivity, which is the local addition of photons to a beam, and the absorption, local removal of photons from a beam. It is thus a measure of how much a medium "shines by itself". In the stellar case the medium is the photosphere. In local thermodynamic equilibrium (LTE) the source function equals the Planck function and thus only depends on the temperature. In LTE, the population of electrons in a certain excitation level, N_n, compared to the total number of atoms of that species, N, is given by the Boltzmann equation

$$\frac{N_n}{N} = \frac{g_n}{u(T)} e^{-\chi_n/kT}, \tag{2.1}$$

where g_n is the statistical weight of the level 2J+1 for the quantum number of the total angular momentum J, $u(T) = \sum g_i e^{\chi_i/kT}$ is the partition function, χ_n is the excitation potential, k the Boltzmann factor and T the effective temperature. The population of an

ionisation stage, N_1, as a ratio of neutral atoms, N_0, is given by the Saha equation

$$\frac{N_1 N_e}{N_0} = \frac{(2\pi mkT)^{1.5}}{h^3} \frac{2g_1}{g_0} e^{-\chi/kT}, \tag{2.2}$$

where N_e is the number density of electrons, m is the electron mass, h is the Planck constant, g_i is the statistical weight of the ground level in each ion and χ is the ionisation energy.

The effective temperature is the temperature of a black-body that would have the same luminosity per surface area as the star. It is used as a measure of the surface temperature. The effective temperature is defined by the Stefan-Boltzmann law

$$F = \sigma T_{eff}^4, \tag{2.3}$$

where F is the flux and σ is the Stefan-Boltzmann constant. A direct mapping from the source function to the flux can be made in LTE, and since the temperature as well as the source function decreases outwards in stars, absorption lines are formed. In non-LTE (NLTE) the relation is not as simple. S_ν is not only dependent on the temperature any more and the mapping cannot be made. LTE is valid where atomic transitions due to collisions dominate over radiative transitions. Then energy is transferred quickly and thermal equilibrium is achieved in at least small regions i.e., local thermodynamic equilibrium. This is accurate in the interior of stars, but in the outer layers of the photosphere this no longer holds since the density is too low and radiation can escape through the surface. Strong lines are not formed at one defined depth, the wings are formed deep in the photosphere (LTE) while the core of the spectral line is formed higher up where LTE is no longer valid.

The strength of a line, the equivalent width (EW), corresponds to the width of a rectangle with the height of the continuum and area equal to that of the spectral line. The line strength depends on the number of absorbers producing the line and the width on the absorption coefficient (a function of thermal and microturbulence velocities). A strong temperature dependence can be seen in eq. 2.1 and 2.2. This makes the temperature a primary factor in the strength of spectral lines. Additionally, the abundance of the element affects the line strength, i.e. the higher abundance, the larger EW. There are three phases of growth with abundance, for weak lines the relation is linear and the width equals the Doppler width, so for higher abundance the line grows in depth proportional to abundance. For stronger lines the depth is approaching the maximum and the line will start to saturate, which means that the wings grow instead. In this phase small changes in abundance will result in large changes in EW. The third phase is for strong lines, where the wing's optical depth becomes significant in comparison to the continuous absorption coefficient. These phases are represented in a curve of growth, shown in Fig. 2.1.1.

A relation between the abundance and equivalent width is given by

$$\log\left(\frac{EW}{\lambda}\right) = \log A + \log C + \log gf\lambda - \theta_{ex}\chi - \log \kappa_\nu, \tag{2.4}$$

where A is the abundance, g and f are the statistical weight and oscillator strength of the atomic level respectively, θ_{ex} is the excitation temperature, χ is the excitation potential

and κ_ν is the opacity of the continuum processes. C is a constant for a given star and ion.

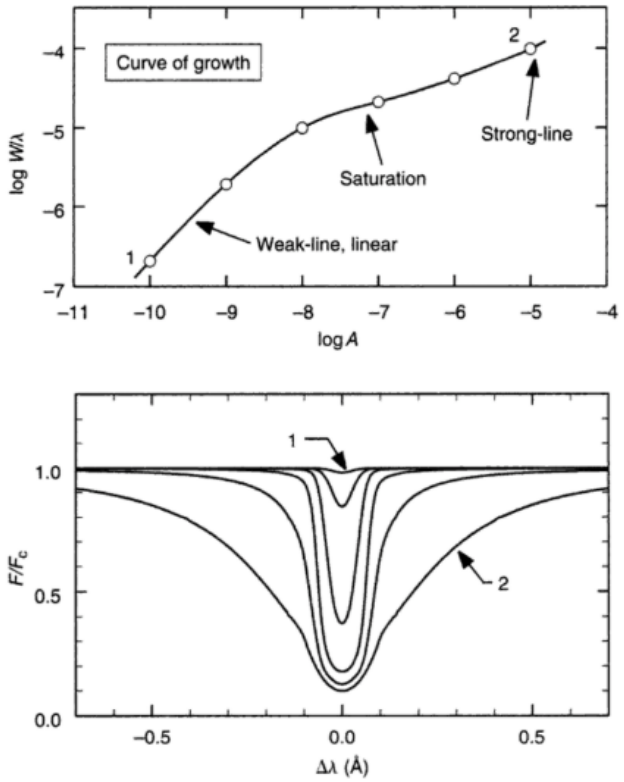

Figure 2.1.1: A curve of growth (upper panel), shows how the equivalent width of a spectral line depends on the abundance. The lower panel shows how the spectral line profile changes, the different lines corresponds to the dots on the curve of growth (Gray 2005).

When applying a differential analysis, the abundance of two stars are compared line-by-line, between a reference star and a star of unknown composition. The reference star is chosen so that the two stars are as similar as possible, in that way the differences of the constants in eq. 2.4 are minimised as well as g, f, λ and χ being the same for each line.

The corresponding formula to eq. 2.4 for differential analysis is just a combination of each star's individual formula,

$$\log \frac{A}{A_{ref}} = \log \frac{EW}{EW_{ref}} + \log \frac{\kappa_\nu}{\kappa_\nu^{ref}} + (\theta_{ex} - \theta_{ex}^{ref})\chi, \tag{2.5}$$

where the sub/superscript ref indicate the reference star. Due to the strong similarity of the stars, the systematic errors and uncertainties in the atomic constants are nearly equal, which allows the total error in the final result to be small.

2.2 Data

The stars in my sample were the Sun, a solar twin HIP 79672 (18 Sco) and two HD stars, HD 102117 and HD 90722. For the Sun, two spectra were used, one that was reflected from the asteroid Juno and one from the asteroid Hebe.

The solar spectra reflected from Hebe was obtained from the 10 m Keck I telescope, with the spectrometer HIRES in January 2015 (Liu et al. 2016a). The spectra had a high resolution of $R = \lambda/\Delta\lambda$=50 000 and high signal to noise ratio (SNR) of $\approx$ 450 per pixel. The wavelength coverage was almost complete in the 400 to 800 nm range.

The other solar spectrum, a reflection of the asteroid Juno, as well as the spectrum for HIP 79672, were obtained with VLT in August 2009, using the spectrograph UVES (Meléndez et al. 2014). The wavelength coverage was almost complete in the range 306-1020 nm, except for two small missing regions, 387-480 and 577-585 nm. In the red arm (480-1020 nm) the achieved resolution was R=110 000 and SNR$\approx$800 per pixel. In the blue arm (306-387 nm) the resolving power was R=65 000 and SNR about 600 per pixel.

The spectra for HD 102117 and HD 90722 were observed at the 6.5 m Clay Magellan telescope using the MIKE spectrometer (Melendez et al. 2009). High resolution (R=65 000) and high SNR ($\approx$ 450 per pixel) were obtained in the 340-1000 nm range.

The line lists were mainly obtained from Grevesse et al. (2015), Scott et al. (2015a) and Scott et al. (2015b) with complements from Reddy et al. (2003), Bensby et al. (2005), Ramírez et al. (2007) and Neves et al. (2009). Not all lines where measurable in each spectrum so the final line lists are not identical for the two stellar sets, but the measured lines are the same within each set to make a line-by-line analysis possible.

2.3 Stellar Parameters

In order to determine the stellar parameters (T_eff: effective temperature, $\log g$: surface gravity, [Fe/H]: metallicity and ξ_{micro}: microturbulence), equivalent widths (EW) for a number of iron-lines were measured with the `splot` task in IRAF. The lines were fitted with gaussian curves and from that the EW was derived for each line. Spectral lines with EW larger than 120 mÅ were discarded to avoid using saturated lines.

To check that there was no systematic offset in EWs measurement, a comparison between this work and Liu et al. (2016a) can be seen in Fig. 2.3.1. The mean difference is $m = -0.345$ mÅ with a standard deviation $\sigma = 2.532$.

A 1D LTE (local thermodynamic equilibrium) abundance analysis was performed, using `MOOG` version 2014 (Sneden 1973). The code fits abundances to yield the same equivalent widths, in equation 2.4, as the measured ones. For the model atmosphere, ODFNEW grid of Kurucz model atmosphere (Castelli & Kurucz 2003) was used. These model atmospheres assume LTE (discussed in section 2.1), hydrostatic equilibrium and plane-parallel atmospheres. Hydrostatic equilibrium implies that there is no large scale struc-

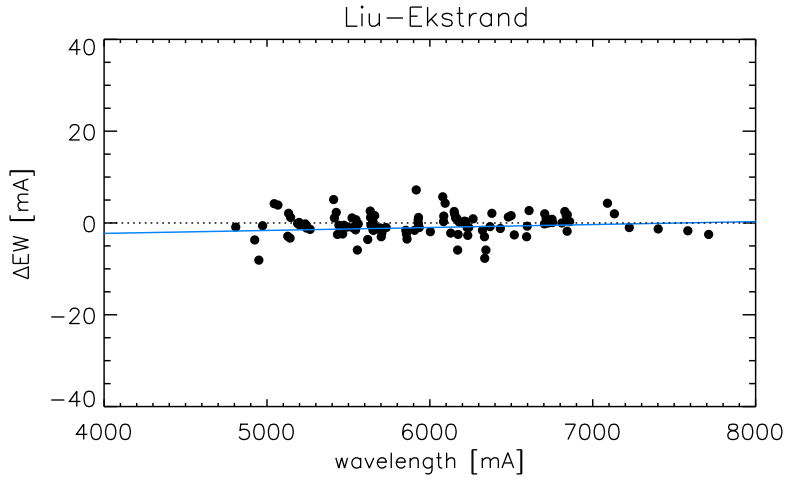

Figure 2.3.1: Comparison of the measurements of equivalent widths for iron lines (used for determination of stellar parameters) for Sun(Hebe), between Liu et al. (2016a) and this project. The blue line is the least square fit to the data and has a slope of $(0.03\pm0.04)\times10^{-6}$.

tural changes in the star. Plane-parallel atmospheres implies that all physical parameters only depend on the depth in the star so that, for example, each depth has a defined temperature. This is a good approximation if the photosphere is relatively thin in comparison to the star's radius.

To obtain the stellar parameters, an excitation and ionisation balance are required. The effective temperature (T_{eff}) was obtained when the abundance of iron lines showed no dependence on the excitation potential, the surface gravity when the same abundances were given for both FeI and FeII lines, and the microturbulence when the abundances of iron lines were not dependent on the reduced equivalent width ($\log(EW/\lambda)$). The microturbulence is small scale velocities in the star, smaller than the mean free path of the photons that have a broadening effect on the spectral lines.

The temperature enters the Boltzmann equation in a power dependence (eq. 2.1) which is included in eq. 2.4. The derived elemental abundance should not depend on which excitation level the lines come from and therefore the excitation balance is required. In stars of similar temperature as the Sun, iron is mostly ionised. The gravity (pressure) dependence of the abundance from neutral lines is therefore approximately zero. However, the spectral lines originating from ions are sensitive to gravity, having an effect on the equivalent width. The different ionisation stages should yield the same elemental abundance and the surface gravity is thus determined by requiring them to be equal. Microturbulence (ξ_{micro}) has an effect of delaying the saturation in the curve of growth and thereby its effect on the $\log(EW/\lambda) - \log A$ relation.

The stellar parameters where determined in three steps, as described below.

2.3.1 Manually derived stellar parameters

To better understand how the different parameters affect the balancing plots (e.g. Fig. 2.3.2), they where first changed manually. The aim was to get the slopes of the balancing plots to be as small as possible. These plots show the absolute abundance as a function of excitation potential (E.P.) and reduced equivalent width (EW/λ), an example is shown in Figure 2.3.2. For the correct stellar parameters the slopes should be close to zero and the FeI and FeII lines balanced between each other.

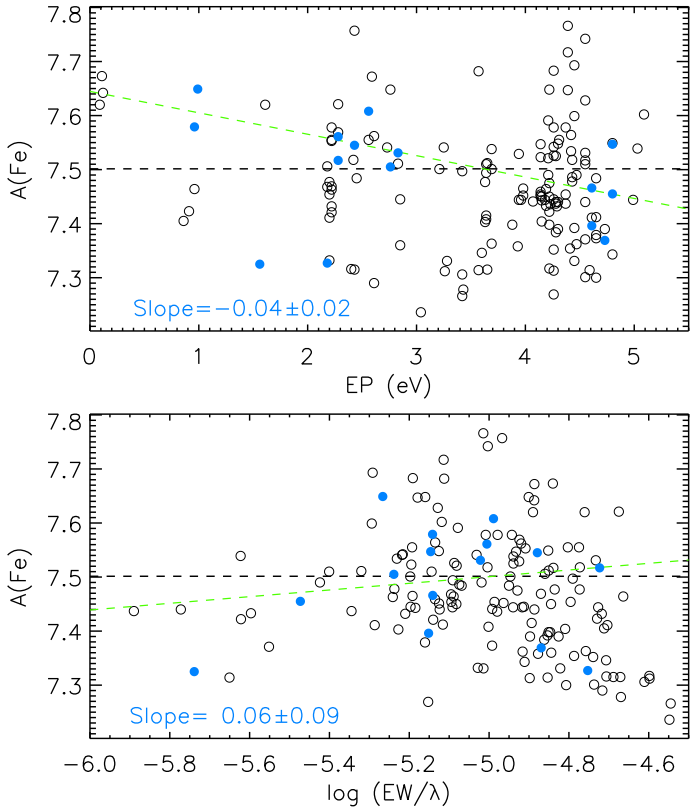

Figure 2.3.2: Example of a balancing plot for wrong stellar parameters. Open and filled circles represent abundances derived from FeI lines and FeII lines respectively, the black dotted line shows the mean abundance and the green dashed line is the linear least square fit to the data.

The manual iteration was carried out, for the five spectra in the sample, until the balancing plots fulfilled the criteria. The resultant stellar parameters for each star can be seen in Table 2.1.

Table 2.1: Absolute stellar parameters, determined manually, for the five stars.

Object	T_{eff} [K]	$\log g$	[Fe/H]	ξ_{micro} [km/s]
Sun(Juno)	5725	4.30	0.00	0.88
Sun(Hebe)	5770	4.40	0.00	1.00
HIP 79672	5810	4.40	0.10	1.00
HD 90722	5670	4.20	0.30	1.10
HD 102117	5640	4.25	0.35	1.05

2.3.2 Automatically determined stellar parameters

Since the iterating work of changing the parameters by hand was very time consuming, an automatic code was implemented instead. More iterations could be made and the parameters were changed until the slopes in the two plots were close to zero, as well as the difference between FeI and FeII. We adopted the parameters listed Table 2.1 as initial guesses. The stellar parameters determined using the automatic code are listed in Table 2.2.

Table 2.2: Absolute stellar parameters, determined automatically, for the five stars.

Object	T_{eff} [K]	$\log g$	[Fe/H]	ξ_{micro} [km/s]
Sun(Juno)	5721	4.29	-0.047	0.84
Sun(Hebe)	5761	4.40	-0.081	1.01
HIP 79672	5764	4.33	-0.016	0.93
HD 90722	5687	4.22	0.337	1.11
HD 102117	5633	4.25	0.292	1.05

2.3.3 Differential stellar parameters

A line-by-line differential approach was used for the final stellar parameters in order to achieve extremely high precision, as described in Meléndez et al. (2012). This means that the abundances of the comparison star is subtracted from the reference star abundances, line-by line as

$$\delta A_i = A_i^{ref} - A_i^{comp}. \tag{2.6}$$

It is the differential ionisation/excitation balance between two stars that are used in the balancing plots to derive the stellar parameters. The temperature is obtained by the excitation equilibrium

$$\frac{\mathrm{d}(\delta A_i^{FeI})}{\mathrm{d}(\chi_{exc})} = 0, \tag{2.7}$$

and the surface gravity is attained by the relative ionisation equilibrium where the mean difference in FeI and FeII respectively are equal,

$$\langle \delta A_i^{FeII} \rangle - \langle \delta A_i^{FeI} \rangle = 0. \tag{2.8}$$

Finally, the microturbulence is derived by not having the abundance dependent on line strength

$$\xi_{micro} = \frac{\mathrm{d}(\delta A_i^{FeI})}{\mathrm{d}(\log(EW/\lambda)).} \tag{2.9}$$

The final stellar parameters were achieved when these three conditions, as well as obtaining the same iron abundance as the input model value were fulfilled. The more similar the stars are, higher precision in the results will be achieved. This is because most of the systematic errors, for example in the atomic constants (gf-value) cancel. Therefore in a differential line-by-line analysis, the accuracy of the atomic constants does not affect our results.

In this final step an automatic grid searching method was applied (Liu et al. 2014) to determine the stellar parameters for the comparison stars. The reference stars of the two sets were chosen to be Juno and HD 90722. For Juno we adopted the standard solar values, seen below. On the other hand the values of HD90722 were discussed in several studies, for example $T_{eff} = 5719$ K, $\log g = 4.31$, [Fe/H] = 0.36 (Valenti & Fischer 2005), $T_{eff} = 5720$ K, $\log g = 4.19$, [Fe/H] = 0.36 (Melendez et al. 2009) and $T_{eff} = 5711$ K, $\log g = 4.28$, [Fe/H] = 0.31 (Sousa et al. 2011), and from these values the following parameters were adopted for the reference stars:
Juno: $T_{eff} = 5777$ K, $\log g = 4.44$, [Fe/H] = 0.00, $\xi_{micro} = 1.00$ km/s
HD 90722: $T_{eff} = 5720$ K, $\log g = 4.19$, [Fe/H] = 0.36, $\xi_{micro} = 1.00$ km/s.

The initial guesses for the comparison stars are listed in Table. 2.2. For HIP 79672 we reset the initial guess to be $T_{eff} = 5821$ K, $\log g = 4.49$, [Fe/H] = 0.04, $\xi_{micro} = 1.06$ km/s (Meléndez et al. 2014) and for HD 102117 to be $T_{eff} = 5700$ K, $\log g = 4.27$, [Fe/H] = 0.32, $\xi_{micro} = 0.95$ km/s (Melendez et al. 2009).

Around the initial guesses of T_{eff}, $\log g$ and ξ_{micro} for the comparison stars, a grid of 5x5x5 points were created. In these points the parameters were changed one by one to get 125 sets of stellar parameters. The abundances and balancing plots were calculated for each set of parameters and the best combination was selected. This was then repeated a number of times while the grid step size was halved each time. The new initial guess was taken to be the best result from the previous iteration. The final parameters were obtained when the grid step size had been reduced to $\Delta T_{eff} = 1$ K, $\Delta \log g = 0.01$ cm s^{-2}, $\Delta\xi_{micro} = 0.01$ km s^{-1}. The derived averaged iron abundance was required to be equal to the input model value.

The final stellar parameters are listed in Table 2.3 and 2.4. The errors in the stellar parameters are listed together with the result. They are estimated using the method described in Epstein et al. (2010) and Bensby et al. (2005), and will be described more thoroughly in section 2.5.

The balancing plot for HIP 79672 relative to the Sun(Juno) can be seen in Figure 2.3.3. It is an example when the stellar parameters were determined, slopes very close to 0 with FeI and FeII centred relative to each other. The corresponding balancing plot for the HD stars is shown in Fig. 2.3.4. The linear fits (green dashed line) in these figures are not weighted by the error in the data.

Table 2.3: Differential stellar parameters for the Sun(Hebe) and its solar twin. Sun(Juno) is the reference star, so its parameters were fixed.

Object	T_{eff} [K]	$\log g$	[Fe/H]	ξ_{micro} [km/s]
Juno*	5777	4.44	0.000	1.00
Hebe	5807 ± 17	4.48 ± 0.03	-0.026 ± 0.011	1.15 ± 0.03
HIP 79672	5821 ± 12	4.49 ± 0.02	0.040 ± 0.009	1.06 ± 0.02

*reference star

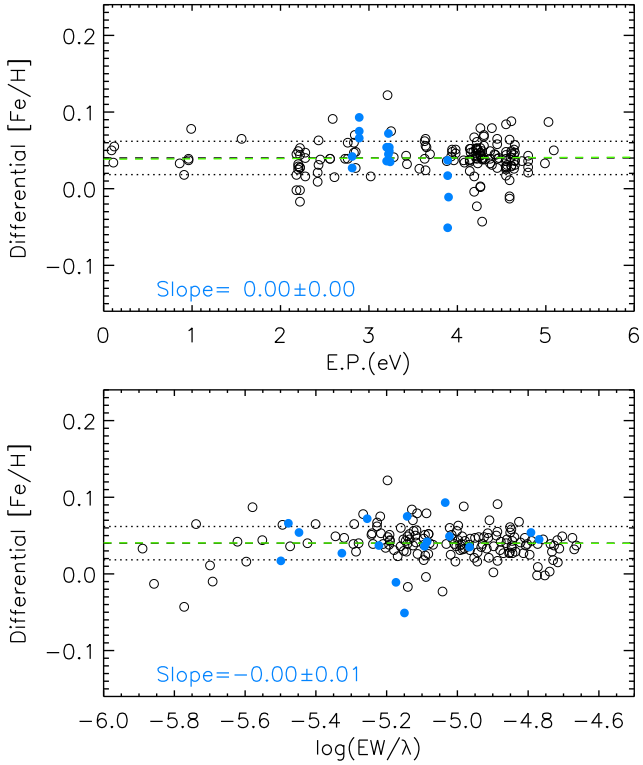

Figure 2.3.3: Example of a balancing plot when stellar parameters were determined, in this case HIP 79672 relative to the Sun(Juno). Open and filled circles represent differential abundances of FeI lines and FeII lines, respectively. The black dashed line shows the mean abundance,the dotted lines are $\pm 1\sigma$ and the green dashed line the linear least square fit to the data.

Table 2.4: Differential stellar parameters for the HD-stars. HD 90722 is the reference star, so its parameters were fixed.

Object	T_{eff} [K]	$\log g$	[Fe/H]	ξ_{micro} [km/s]
HD 90722*	5720	4.19	0.360	1.00
HD 102117	5686 ± 15	4.23 ± 0.029	0.305 ± 0.012	0.99 ± 0.031

*reference star

We also derived the stellar parameters of HD 90722 and HD 102117, relative to the Sun (Juno) and listed the results in Table 2.5.

Table 2.5: Differential stellar parameters for HD 90722 and HD 102117, relative to the Sun

Object	T_{eff} [K]	$\log g$	[Fe/H]	ξ_{micro} [km/s]
Sun(Juno)*	5777	4.44	0.00	1.00
HD 90722	5748 ± 37	4.37 ± 0.063	0.366 ± 0.021	1.25 ± 0.073
HD 102117	5704 ± 34	4.40 ± 0.063	0.314 ± 0.020	1.22 ± 0.071

*reference star

We note that the errors are larger in this comparison than in the preceding ones, due to the fact that the HD-stars are slightly cooler and more metal rich than the Sun. Thus the systematic errors do not cancel.

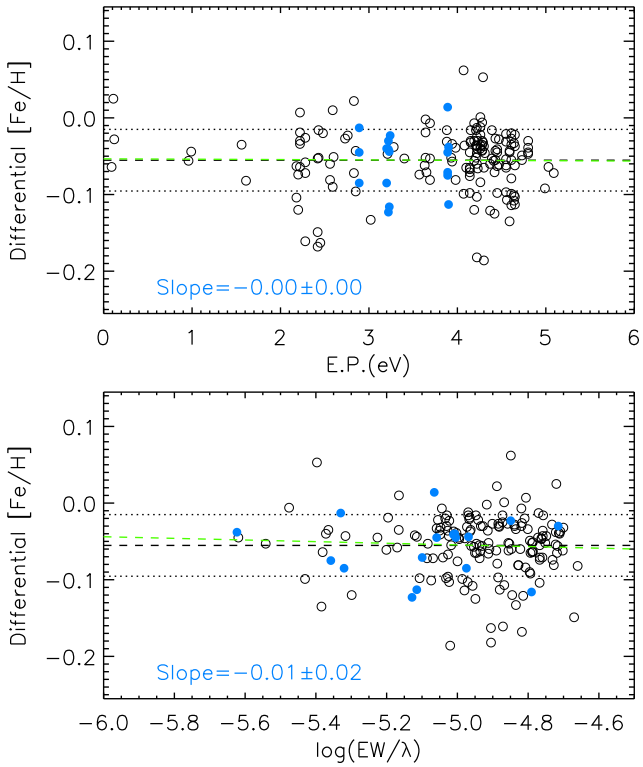

Figure 2.3.4: Example of a balancing plot when stellar parameters were determined, in this case HD 102117 relative to HD 90722. Open and filled circles represent differential abundances of FeI lines and FeII lines, respectively. The black dashed line shows the mean abundance, the dotted lines are $\pm 1\sigma$ and the green dashed line the linear least square fit to the data.

2.4 Differential chemical abundance analysis

A line-by-line differential abundances analysis was conducted. We recall that the comparison stars have to be almost identical to the reference stars in our line-by-line differential analysis, so that the systematic errors actually cancel.

The equivalent width of spectral lines for other elements than iron, were measured. A comparison of EW measurement between this work and Meléndez et al. (2014), is shown in Fig. 2.4.1. The mean difference is $m = -0.784$ mÅ and standard deviation $\sigma = 1.787$ mÅ. No significant systematic offset between the EW measurements were identified.

The differential abundances between the reference and comparison stars were calculated with the IDL-pipeline by Liu et al. (2014). The absolute abundance was calculated for each line in all the stars and then the values for the reference star were subtracted from the comparison star line-by-line.

3D NLTE corrections were made for the oxygen-triplet (777.1 nm, 777.4 nm, 777.5 nm) in all the stars based on Amarsi et al. (2015). For HD 90722 and HD 102117, the corrections were of the order -0.26 while for the Sun and HIP 79672 the corrections were smaller, around -0.17.

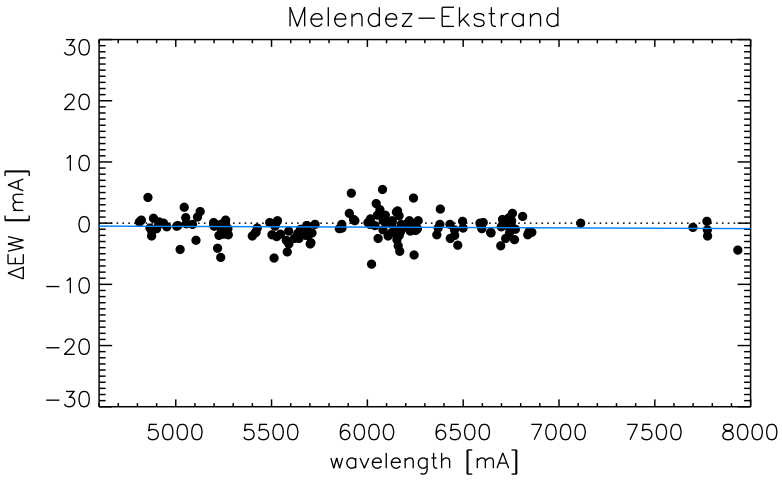

Figure 2.4.1: Comparison of the measurement of equivalent widths of HIP 79672 for all elements, between Meléndez et al. (2014) and this project. The blue line is the least square fit to the data with a slope of $(0.26\pm0.24)\times10^{-5}$.

2.5 Error analysis

The method for the error analysis was taken from Epstein et al. (2010) and Bensby et al. (2014). The errors were calculated from how uncertainties propagate in three observables, used to determine the stellar parameters. The first, o_1, corresponds to the slope of the linear fit in the abundance-EP balancing plot, the second, o_2, to the slope of the linear

fit in the abundance-log(EW/λ) balancing plot and the third to the difference between abundances of FeI and FeII. In Epstein et al. (2010) they had a fourth observable, the difference between the input model [Fe/H] abundance and the output [Fe/H] abundance. In this work this last one is neglected because those values are required to be equal in the derivation of the stellar parameters and this observable would thus not differ.

The observables were written as linear combinations of the deviations from the best fit model:

$$o_i = o_i^0 + \sum_{j=1}^{3} b_{ij}(m_j - m_j^0), \tag{2.10}$$

where o_i are the observables, m_j are the stellar parameters and the super-index "0" indicate the best fit model. b_{ij} is the partial derivatives of the observables with respect to the stellar parameters, $b_{ij} = \partial o_i/\partial m_j = \Delta o_i/\Delta m_j$, and the values are determined by varying the value of one stellar parameter at a time. The amount of change, Δm_j, for the different parameters are set to $\Delta m_1 = 80$ K, $\Delta m_2 = 0.05$ dex and $\Delta m_3 = 0.05$ km/s.

New abundances could be calculated when changing stellar parameters and thus the observables changed in comparison to the best fit model, o_i^0. Equation 2.10 then results in a number of equations that can be solved. Each observable has an error σ_k, and the errors in the stellar parameters, $\sigma(m_j)$, can be solved for as

$$\sigma(m_i) = \sqrt{\sum_{k=1}^{3} c_{ik}^2 \sigma_k^2}, \tag{2.11}$$

where c_{ik} is the inverted b_{ij}-matrix. The errors in the first two observables, σ_1 and σ_2, represent the uncertainty in the linear fits in each plot, and the third error, σ_3, is connected to the errors in FeI and FeII abundances. The errors calculated by equation 2.11 can be seen together with the stellar paramters in Table 2.3 and 2.4.

Concerning the errors in the differential abundances, the method was very similar as for the stellar parameters. The abundances (X) were written as linear combinations of deviations from the best fit model as

$$X = X_0 + \sum_{j=1}^{3} \kappa_j(m_j - m_j^0) = X_0 + \sum_{j=1}^{3} \alpha_j(o_j - o_j^0), \tag{2.12}$$

where $\alpha_j = \sum_{j=1}^{3} \kappa_k \cdot c_{kj}$ and $\kappa_j = \Delta X/\Delta m_j$, which was calculated by changing the stellar parameters as described before.

The errors for the measured average abundances were then calculated by

$$\sigma_X = \sqrt{\sigma_{X_0}^2 + \sum_{k=1}^{3} \alpha_k^2 \cdot \sigma_k^2}, \tag{2.13}$$

where σ_k is the error in the observables and σ_{X_0} is the error in the measured abundances.

The error in the abundance ratio between two elements, [X/Y], was then given by

$$\sigma_{XY} = \sqrt{\sigma_X^2 + \sigma_Y^2 - 2\sum_{k=1}^{3} \alpha_{k,X} \cdot \alpha_{k,Y} \cdot \sigma_k^2}. \tag{2.14}$$

The errors in the abundance ratios for all elements were listed together with the measured abundances in Table 3.1.

Chapter 3

Results

A line-by-line differential abundance analysis was carried out for 26 species: C, O, Na, Mg, Al, Si, S, K, Ca, Sc, Ti (I and II), V, Cr (I and II), Mn, Fe, (I and II), Co, Ni, Cu, Zn, Y, Ba, Ce and Eu. The HD stars were compared to each other, with HD 90722 as the reference star, and the solar twin HIP 79672 (18 Sco) was compared to the Sun(Juno). The solar spectra were compared to each other to check if a systematic offsets exist between two instruments (UVES/VLT and HIRES/Keck). The two HD star were compared to the Sun as well. In these three solar cases Sun(Juno) was the reference star. The differential abundances as well as the related uncertainties for these cases are listed in Table 3.1 and 3.2.

To check that there was no systematic offset between two instruments, the solar spectra from the asteroids Juno (taken at VLT) and Hebe (obtained at KECK) were compared. The result is shown in Fig. 3.0.1, where the differential abundances, Δ[X/H] are plotted against the 50 % condensation temperature from Lodders (2003). This is the temperature where 50% of the element has condensed to solid form. For this and the following figures a linear least square fit to the data was made, weighted by the errors in the derived abundances. The average abundance difference between the two spectra was m=-0.017 dex and the mean error of the data σ=0.019 dex. The slope of the linear fit is $(-0.69 \pm 0.96) \times 10^{-5}$ K^{-1}, and a dispersion (standard deviation) around the linear fit of $\sigma_s = 0.023$. We only had one line for Eu in our line list and it was hard to measure, this is why the abundance of this element differs. Scandium (Sc) seems to differ between the stars because hyperfine splitting (HFS) is not taken into account in this work. HFS comes from odd nucleon numbered nuclei, in which the total angular momentum is not zero and alters the energy levels of the electrons. This has a broadening effect in the line profiles. We note that the oxygen abundance slightly differs. We conclude that no systematic offset was found within errors, when comparing solar spectra taken with UVES/VLT and HIRES/Keck.

In Fig. 3.0.2 the abundance differences between the solar twin HIP 79672 and the Sun is shown. The result from Meléndez et al. (2014), for the common elements, is plotted as blue triangles. The slope of the linear fit is $(5.21 \pm 0.77) \times 10^{-5}$ K^{-1}, which is significant at 6.8-σ level. There is a trend for increasing differential abundance for higher conden-

sation temperature. Thus the refractory elements are more abundant in the non-planet hosting solar twin than in the Sun, which agrees well with the results by Meléndez et al. (2014).

Table 3.1: Differential abundances and errors for the compared stars, where X is the species.

	HD 102117-HD 90722		HIP 79672-Juno		Hebe-Juno	
Species	Δ[X/H]	$\sigma[X/H]$	Δ[X/H]	$\sigma[X/H]$	Δ[X/H]	$\sigma[X/H]$
C	-0.039	0.0282	-0.023	0.0229	0.007	0.0213
O	-0.030[a]	0.0342	0.012[a]	0.0217	-0.040[a]	0.0265
Na	-0.095	0.0323	0.023	0.0065	0.003	0.0104
Mg	-0.038	0.0137	0.029	0.0064	0.009	0.0142
Al	-0.024	0.0063	0.031	0.0165	0.012	0.0123
Si	-0.056	0.0084	0.050	0.0049	0.002	0.0086
S	-0.092	0.0169	-0.004	0.0173	-0.031	0.0242
K	-0.051	0.0310	0.008	0.0305	-0.019	0.0311
Ca	-0.019	0.0125	0.052	0.0066	-0.029	0.0114
Sc	-0.086	0.0175	0.062	0.0095	-0.046	0.0172
TiI	-0.017	0.0141	0.059	0.0095	-0.004	0.0143
TiII	-0.039	0.0205	0.069	0.0130	-0.010	0.0179
V	-0.045	0.0171	0.051	0.0121	0.005	0.0194
CrI	-0.025	0.0170	0.056	0.0105	-0.011	0.0187
CrII	-0.017	0.0207	0.053	0.0120	-0.041	0.0254
Mn	-0.091	0.0288	0.030	0.0081	-0.009	0.0132
FeI	-0.055	0.0115	0.040	0.0092	-0.026	0.0110
FeII	-0.055	0.0343	0.040	0.0203	-0.026	0.0258
Co	-0.072	0.0216	0.044	0.0149	0.004	0.0161
Ni	-0.068	0.0091	0.045	0.0067	-0.002	0.0092
Cu	-0.103	0.0449	0.024	0.0155	-0.002	0.0183
Zn	-0.049	0.0306	0.042	0.0423	-0.026	0.0249
Y	-0.038	0.0199	0.078	0.0199	0.030	0.0199
Ba	-0.029	0.0172	0.092	0.0091	-0.042	0.0144
Ce	-0.058	0.0326	0.200	0.0315	0.024	0.0331
Eu	-0.074	0.0322	0.108	0.0313	-0.059	0.0327

[a] NLTE abundances

Most elements show similar differential abundances between this work and Meléndez et al. (2014). Eu is the only outlier, as discussed before, only one blended line was available and that made it hard to measure. Also zinc (Zn) and potassium (K) slightly differ, although within the errors. Potassium was measured using only one strong line which is likely saturated.

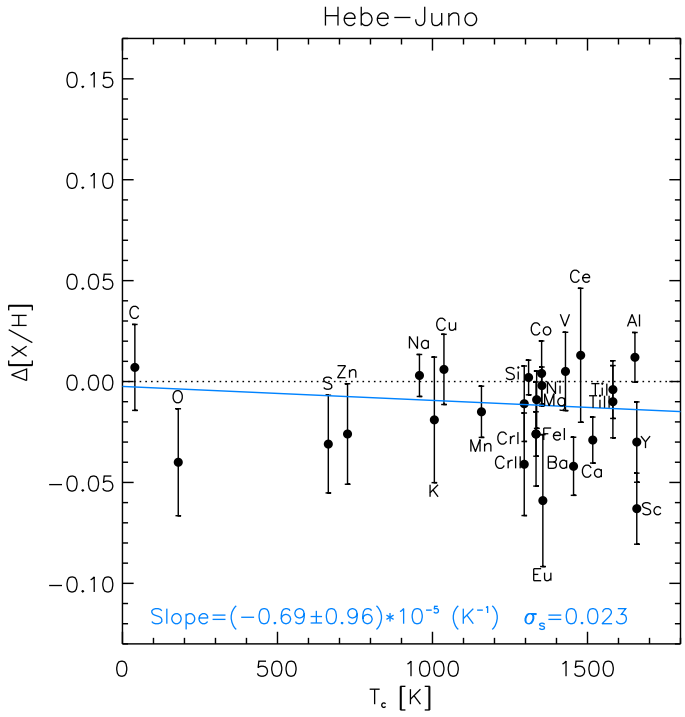

Figure 3.0.1: The differential abundances of Hebe in comparison to Juno. The blue solid line is the linear least square fit to the data. σ_s is the dispersion about the linear fit.

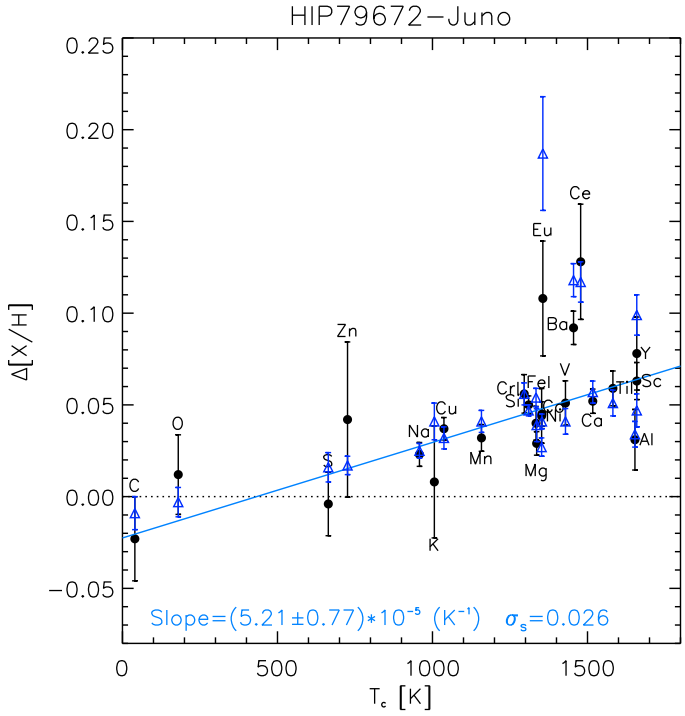

Figure 3.0.2: The differential abundances of HIP 79672 in comparison to Juno. The black filled circles are values from this project and the triangles are values from Meléndez et al. (2014). The blue solid line is the linear least square fit to the data (circles). σ_s is the dispersion about the linear fit.

In Meléndez et al. (2014) the neutron capture elements are much more abundant in HIP 79672 than in the Sun. Neutron capture elements are those with a higher atomic mass than 56, i.e. larger atomic number than 26. These elements can not be created in nuclear fusion, but only by absorbing one or many neutrons and then go through β^- decay to a higher atomic number. Several common neutron capture elements (Co, Ni, Cu, Zn, Y, Ba, Ce, Eu) are included in this work, and show similar enrichment except for Eu (most likely due to the limitation of measurable lines in our spectral regions).

The derived differential abundances for the HD stars compared to the Sun can be seen in Table. 3.2 and are shown in Fig. 3.0.3. The black dotted lines are the difference in iron abundance between the HD stars and the Sun respectively. HD 90722 has no known planet and shows no clear trend to the Sun except having higher overall metallicity. Neither is a trend evident for HD 102117, which seems reasonable since no trend was found when comparing the two HD stars to each other (Fig. 3.0.4). The mean difference in abundance in the left panel is 0.327 dex with mean error 0.038 dex, and for the right panel the mean is 0.380 dex with mean error of 0.040 dex.

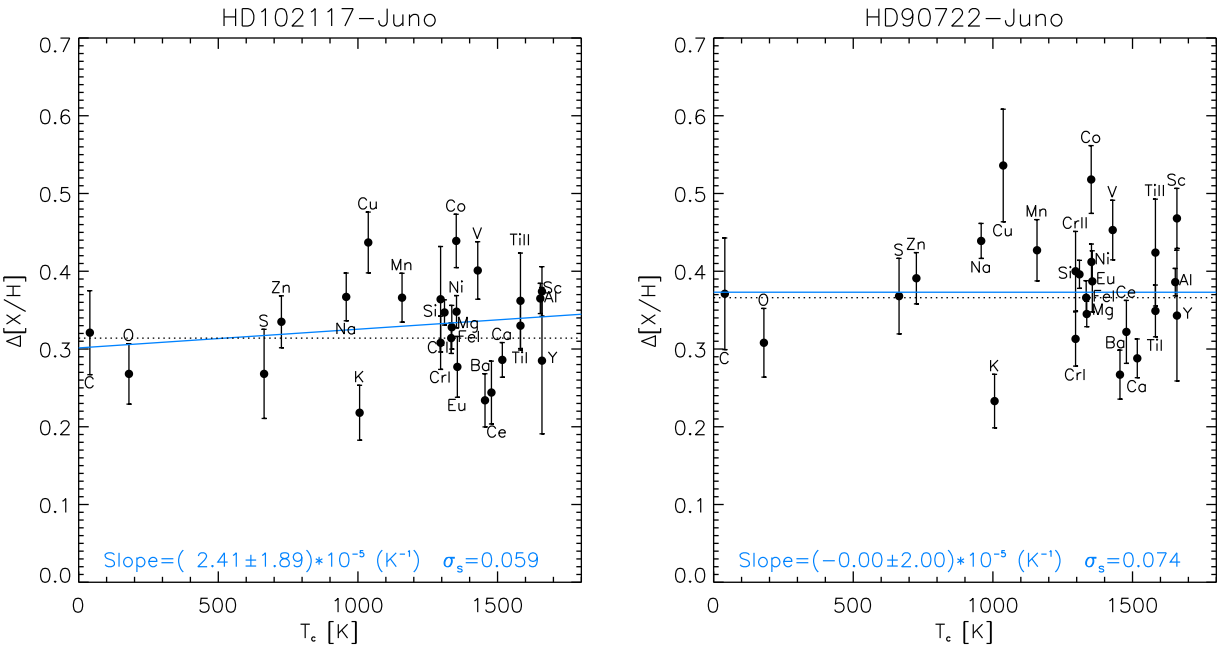

Figure 3.0.3: Left panel: the differential abundances of HD 102117 in comparison to Juno(Sun). Right panel: the differential abundances of HD 90722 in comparison to Juno. The blue solid line is the linear least square fit to the data and the black dotted line is Δ[Fe/H] between the stars. σ_s is the dispersion about the linear fit.

Since the reference star (Sun) is not as similar to the comparison stars (HD 90722 and HD 102117) in this case as in the previous ones, the errors are larger. The slope of the linear fits are $(2.41 \pm 1.89) \times 10^{-5}$ K^{-1} and $(-0.00 \pm 2.00) \times 10^{-5}$ K^{-1} respectively, which are not significant. The dispersion around the linear fit is larger than in previous cases as well. We did not see any special chemical pattern for both HD stars relative to the

Sun due to the large uncertainties. It is thus unclear whether a star with a hot Jupiter behave differently from a star with a cold Jupiter.

Table 3.2: Differential abundances and errors for the HD-Sun star comparison, where X is the species.

	HD 102117-Juno		HD 90722-Juno	
Species	Δ[X/H]	$\sigma[X/H]$	Δ[X/H]	$\sigma[X/H]$
C	0.321	0.0540	0.371	0.0718
O	0.268[a]	0.0389	0.0308[a]	0.0442
Na	0.367	0.0307	0.439	0.0225
Mg	0.328	0.0281	0.345	0.0163
Al	0.365	0.0194	0.386	0.0176
Si	0.347	0.0162	0.396	0.0180
S	0.268	0.0573	0.368	0.0486
K	0.218	0.0353	0.233	0.0344
Ca	0.286	0.0223	0.288	0.0249
Sc	0.374	0.0319	0.468	0.0386
TiI	0.330	0.0313	0.349	0.0333
TiII	0.362	0.0614	0.424	0.0687
V	0.401	0.0370	0.453	0.0383
CrI	0.308	0.0342	0.313	0.0350
CrII	0.364	0.0678	0.400	0.0512
Mn	0.366	0.0314	0.427	0.0394
FeI	0.314	0.0197	0.366	0.0219
FeII	0.314	0.0481	0.366	0.0440
Co	0.439	0.0343	0.518	0.0436
Ni	0.348	0.0207	0.412	0.0230
Cu	0.437	0.0391	0.536	0.0724
Zn	0.335	0.0334	0.391	0.0330
Y	0.285	0.0941	0.343	0.0841
Ba	0.234	0.0342	0.267	0.0315
Ce	0.244	0.0404	0.322	0.0405
Eu	0.277	0.0319	0.387	0.0393

[a] NLTE abundances

The two stellar twins, HD 102117 and HD 90722, were compared to each other with HD 90722 as the reference star. The result is shown in Fig. 3.0.4. From the data there is no clear trend with the condensation temperature, but it is clear that the planet-hosting HD 102117 is depleted in all elements compared to HD 90722, which has no known planets. The mean difference of all elements is seen as the red dash-dotted line in the Δ[X/H] plot, and has a value of approximately -0.05 dex and the mean error is 0.027 dex. For the elements with $T_C \geq 900$ K, an increase in differential abundance with condensation temperature can be seen. Subtracting the iron-abundance from all other elements, the abundances are normalised to 0, which is seen in the right panel of Fig. 3.0.4.

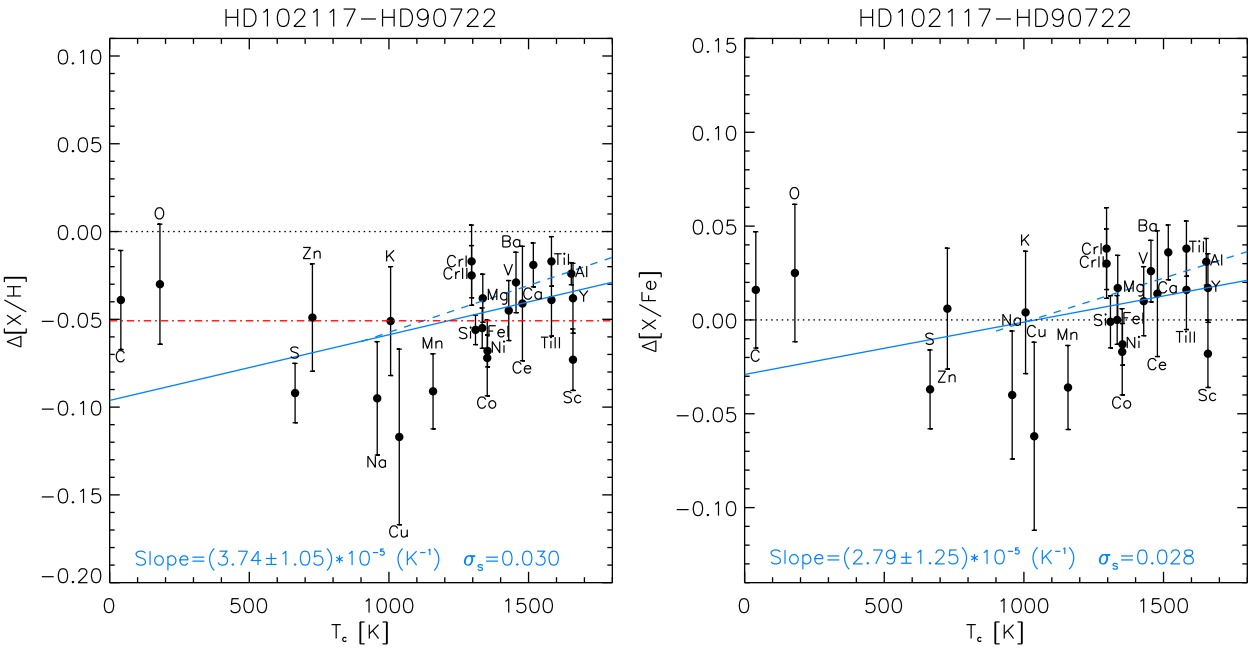

Figure 3.0.4: The differential abundances of HD 102117 in comparison to HD 90722. The left panel shows Δ[X/H] and the right panel Δ[X/Fe] as functions of condensation temperature. The blue solid line is the linear least square fit to the data, the blue dashed line is the linear fit to elements with $T_C \leq 900$ K and the red dashed-dotted line is the mean abundance difference between the two stars. σ_s is the dispersion about the linear fit.

The slopes of the linear fit in the two panels (blue solid line) are positive with values: $(3.74 \pm 1.05) \times 10^{-5}$ K^{-1} in the left panel and $(2.79 \pm 1.25) \times 10^{-5}$ K^{-1} in the right respectively. When calculating the linear fit, it is weighted by the errors in each element. The errors for some of the refractories are small, smaller than the volatiles, and therefore the elements with higher condensation temperature gives a larger contribution to the fit. When removing the weighting of the linear fits for all elements (solid lines), the slopes became equal and zero within the errors ($(1.26 \pm 1.32) \times 10^{-5}$ K^{-1}). The dashed blue lines show the linear fit to elements with $T_C \geq 900$ K, $(8.01 \pm 1.87) \times 10^{-5}$ K^{-1} and $(7.06 \pm 2.41) \times 10^{-5}$ K^{-1} for the left and right panel respectively. The dashed lines on the other hand did not change significantly when removing the weighting and thus an increase with condensation temperature is seen if only those elements are considered. The planet host HD 102117 shows an overall deficiency in comparison to its stellar twin, HD 90722, by about 0.05 dex. Further, a positive trend with condensation temperature is detected for the refractory elements with T$_c$ $\geq$900 K at a 4-σ significance level.

We note that Cu is an outlier with errors (0.0449 dex) much larger than the average errors of other elements (0.0211 dex). It is because the copper lines where hard to measure due to an uneven continuum and blending.

Chapter 4

Discussion

A line-by-line differential abundance analysis of four stars using five spectra has been conducted. The comparison of Hebe to Juno, as well as HIP 79672 to Juno (with comparison to Meléndez et al. (2014)), was conducted in order to check whether the results of my work were robust. No systematic offsets were found between the two different spectrographs. My results (HIP 79672 to Juno) agree well with Melendez et al. (2014).

When comparing the abundances of the two HD stars to the Sun, no T_C-trend was identified. No other feature was clear either so the result was mainly an offset in metallicity due to that the HD stars are more metal rich than the Sun. Both stars show similar chemical abundance pattern to the Sun. The errors in this comparison are very large due to that the stars are not as similar, which make it hard to draw any conclusions.

The main result in this study is the comparison between the stellar twins (almost identical stellar parameters), HD 102117 and HD 90722, where the former is a giant planet host. HD 102117 is of about the same mass as the Sun but it is bigger, with a radius of 1.27 $R_\odot$ (Exoplanet.eu). The planet around it is found to have a minimum mass of 0.172 ± 0.018 M_J (Jupiter mass), and is closer to its host star, 0.15 au (Exoplanet.eu) than Jupiter is to the Sun. This is the only found planet in the system and no planet has been found around HD 90722 either. HD 90722 is similar to HD 102117 in mass as well as in size, 1.25 $R_\odot$ (Takeda et al. 2007).

A similar comparison as in this work, is the comparison of the two components in the binary system 16 Cygni. Several papers discuss this binary system, Schuler et al. (2011), Tucci Maia et al. (2014) and Ramírez et al. (2011). Also here, only one planet has been found, around the secondary star 16Cyg B, while none is detected around the primary. Although the HD stars are not a binary, the system 16 Cygni has some similar features as the HD stars. The advantage of examining a binary is that both components are assumed to have formed from the same stellar cloud and therefore have the same initial chemical composition. Any abundance differences should have appeared during, or after, the stars were formed. Schuler et al. (2011) found no trend or offset, between the stars, saying that they are identical. Ramírez et al. (2011) found that 16Cyg A is in general 0.04 dex more metal rich than its planet hosting companion, and Tucci Maia et al. (2014) in addition

to an overall offset also found a trend with condensation temperature for the refractory elements. The study by Schuler et al. (2011) have larger uncertainty and a differential analysis was not conducted, so the focus will be on the other two studies. The different result could be explained by the different resolution and signal to noise ratios for the two observations. In Ramírez et al. (2011) the SNR is about 300-500 per pixel and the resolving power R=60 000. Tucci Maia et al. (2014) had a very large resolution of R=81 000, and a SNR of 700 per pixel. This indicates that with higher resolution, a more detailed analysis of stars with more signatures showing might be obtained.

The resolving power and SNR in this work, for the HD stars, are about the same as in Ramírez et al. (2011), and both comparisons yield similar result: an overall offset in metallicity between the stars. The difference in average abundance for the HD stars is about 0.05 dex while for 16 Cygni it is 0.04 dex. The minimum mass of the planet around 16Cyg B is much larger than HD 102117b, but the metallicity offset in the stars are found to be similar, although the stars are of similar mass and size. A difference in the size of the convective zones of the host stars at the time of accretion could explain this. The same depletion in the nebula would give a smaller effect in a larger CZ since the mass held up in the planet is small in comparison to the mass of the CZ. When finding signatures, they only differ in a few percent, so with larger convective zones the difference will be even smaller and very hard to detect. Also, even though no more planets have been detected around the HD stars, it can not be ruled out that they just have not been found yet.

Usually, giant planets are known to yield an overall offset in metallicity in its host star, coming from that it supposedly contain about equal fractional amounts of refractories and volatiles as the host star (Ramírez et al. 2011). But since the composition of planet interior are not well known, it is a non confirmed assumption. With the higher precision observations in Tucci Maia et al. (2014) they found a trend with condensation temperature, which is usually considered as a terrestrial planet signature. Since no such planet has been discovered, they attribute the trend to the formation of the giant planet's rocky core. Considering the estimated minimum mass, the planet in the 16 Cygni system is much more massive than the planet around HD 102117, 1.5 M_J (Cochran et al. 1997) compared to 0.17 M_J, while the two host stars are of about the same size. A T_c-trend with 4-σ significance level was found for the refractory elements, with $T_c \geq 900$ K, in HD 102117. The trend is less clear and significant than Tucci Maia et al. (2014) because either the planet in HD 102117 is too small to imprint a clear T_C-trend, or my spectra have relatively lower quality. The reason for the trend with condensation temperature is unclear, but it could be due to the rocky core of the planet or a missing terrestrial planet as well as differences in the initial chemical composition of the proto-stellar cloud. A terrestrial planet consist of mainly rocky material and if they where prevented from being accreted onto the Sun a depletion could be noticeable. This planet could then be ejected from the system, in that case the star would still be depleted but no terrestrial planets would be present. In the case of the rocky core of a giant planet, this would also hold up refractory elements and possibly give a T_c trend in the chemical composition.

The difference in metallicity between the two HD stellar twins is possibly due to the planet formation around HD 102117. To estimate what the difference in abundance corresponds

to in mass, the mass of refractories needed to balance out the difference in the convective zone (CZ) was calculated. The chemical composition was scaled to the metallicity of the HD stars using the solar composition (Asplund et al. 2009). The size of the CZ was found in the table[1] from Siess et al. (2000). The mass fractional metallicity Z was taken to be 0.01 (similar to the Sun, which has 0.0135) and two masses were examined, 1 $M_\odot$ from literature[2] and 1.1 $M_\odot$ calculated by Yonsei-Yale isochrones (Yi et al. 2001). The temperature and surface gravity were compared for the different models to see which agreed best with my stellar parameters for HD 102117. For 1 $M_\odot$ the convection zone was found to be 2% and for 1.1 $M_\odot$ 2-3%. These percentages could be even larger, up to 8%. Taking the CZ to be 2% for both stellar masses, the mass of the convective zone was calculated, and then further the mass needed to even out the difference. The material blended into the CZ was an equal mixture of earth-like material and a kind of meteorite material (rich in organic compounds). This method is better for terrestrial planets that show a trend with condensation temperature, than for gas giants since the ratio of the two materials are not known for this type of planets. , For example, the core of Jupiter is hidden under its extensive gaseous envelope and the composition of the core is thus hard to identify. Nevertheless, it is an rough indicator of how much rocky material that is held up in the core of the giant planet or how large a missing terrestrial planet would be.

When mixing 4.1 $M_\oplus$ of each kind of material, in total 8.2 $M_\oplus$, into the CZ (M=1 $M_\odot$) the iron abundance difference becomes small. For the mean abundance of the refractories, $T_c \geq 1100$ K, to be the same, 3.6 $M_\oplus$ of each material was added. For the stellar mass of 1.1 $M_\odot$, 4 $M_\oplus$ of each kind of material was needed to be blended in to show the same average abundance in refractory elements, and 4.5 $M_\oplus$ for the differential iron abundance to be the same. If the CZ of the stars are larger than 2%, which is possible, this mass would become larger. For a convective zone of 5% the missing mass would be 9 $M_\odot$ of each material instead.

The planet around HD 102117 has a minimum mass of 0.17 $M_J \approx 50$ $M_\oplus$. The found missing mass of refractory material, $\approx$ 7-9 $M_\oplus$, could then possibly account for the core of the planet or a missing terrestrial planet. Gas giant's cores are approximately 10 $M_\oplus$ independently of what the total planet mass is. The calculated missing mass and the assumed mass of the core are of the same order of magnitude, keeping in mind that the former is a rough estimate. The offset could also be due to initial differences in the chemical composition of the proto-stellar cloud.

When calculating the mass of the two HD stars, we also determined their stellar ages. HD 102117 was estimated to be around 3.2 ± 1.3 Gyr and HD 90722 3.3 ± 1.6 Gyr, using Yonse-Yale isochrones (Yi et al. 2001). The ages found in literature, for example Takeda et al. (2007), were much higher for these stars, about 8 Gyr. My results ($[\alpha/Fe]$ and other abundance ratios) indicate that these two stars are thin disc stars and might have similar ages to the Sun. The α elements (for example Mg, Ca, Si and Ti) are elements which are produced by combining ^{4}He nuclei. In the HD stars, the $[\alpha/Fe] = [\alpha/H] - [Fe/H]$ are similar to that in the Sun, Table 3.2, which makes my derived stellar ages more reasonable

[1] `http://www.astro.ulb.ac.be/~siess/StellarModels/PMS`

[2] `http://exoplanet.eu/catalog/hd_102117_b/`

than Takeda et al. (2007).

Chapter 5

Conclusions

In this project a line-by-line differential abundance analysis of the Sun, HIP 79672, HD 102117 and HD 90722 was conducted. High resolution, high SNR, spectra were obtained from Keck, VLT and Magellan telescopes.

In order to check that the result is not dependent on the instrument, the solar spectra, obtained from two different telescopes, was compared. No offset was found, thus the two instruments yield the same result. To make sure the final results were robust, a comparison of HIP 79672 and the Sun was done, as in Meléndez et al. (2014). The results show consistency between this work and Meléndez et al. (2014) for the included elements.

The main result obtained was that the planet host HD 102117 is depleted in all elements in comparison to its stellar twin HD 90722 (without known planet). The planet around HD 102117 is a gas giant with a minimum mass of 0.17 $M_{\oplus}$. The average abundance difference was found to be -0.05 dex, and a trend with condensation temperature was identified, although not very clear. It could be that a study with high precision could reveal an even clearer T_C-trend, possibly resulting from the rocky core of the gas planet or a missing terrestrial planet.

A rough estimate for the mass needed to even out the abundance differences between the two HD stars was calculated to 7-9 $M_{\oplus}$. The mass added to the CZ are refractory material and will affect the volatile elements very little. Therefore the average abundance difference of the refractory elements, as well as the differential iron abundance, are used to derive the mass. The stellar age was calculated from isochrones, showing that HD 102117 and HD 90722 are of a similar age as the Sun.

When comparing the HD stars to the Sun, no trend was found. This might indicate that there is no clear dependence of abundance pattern on orbital distance of giant planets, or it can't be detected due to large uncertainties. These two stars are more metal-rich and slightly cooler than the Sun, which make them not ideal for comparison. To further test whether the orbital distance of giant planets has an effect on the chemical composition of its host star, more solar twins with giant planets should be compared to the Sun.

Bibliography

Amarsi, A., Asplund, M., Collet, R., & Leenaarts, J. 2015, MNRAS, 454, L11

Asplund, M., Grevesse, N., Sauval, A., & Scott, P. 2009, ARA&A, 47, 481

Baraffe, I. & Chabrier, G. 2010, A&A, 521, A44

Baraffe, I., Chabrier, G., & Gallardo, J. 2009, ApJ, 702, L27

Bensby, T., Feltzing, S., Lundström, I., & Ilyin, I. 2005, A&A, 433, 185

Bensby, T., Feltzing, S., & Oey, M. 2014, A&A, 562, A71

Buchhave, L., Latham, D., Johansen, A., et al. 2012, Nature, 486, 375

Castelli, F. & Kurucz, R. 2003

Chambers, J. 2010, ApJ, 724, 92

Cochran, W., Hatzes, A., Butler, R., & Marcy, G. 1997, ApJ, 483, 457

Epstein, C., Johnson, J., Dong, S., et al. 2010, ApJ, 709, 447

Exoplanet.eu. (N.d.), HD 102117, `http://exoplanet.eu/catalog/hd_102117_b/`, [Online; accessed 24-April-2017]

Fischer, D. & Valenti, J. 2005, ApJ, 622, 1102

Gonzalez, G. 1997, MNRAS, 285, 403

Gray, D. F. 2005, The observation and analysis of stellar photospheres (Cambridge University Press)

Grevesse, N., Scott, P., Asplund, M., & Sauval, A. 2015, A&A, 573, A27

Liu, F., Asplund, M., Ramirez, I., Yong, D., & Melendez, J. 2014, MNRAS Letters, 442, L51

Liu, F., Asplund, M., Yong, D., et al. 2016a, MNRAS, 463, 696

Liu, F., Yong, D., Asplund, M., et al. 2016b, MNRAS, 456, 2636

Lodders, K. 2003, ApJ, 591, 1220

Melendez, J., Asplund, M., Gustafsson, B., & Yong, D. 2009, ApJ Letters, 704, L66

Meléndez, J., Bergemann, M., Cohen, J., et al. 2012, A&A, 543, A29

Meléndez, J., Ramírez, I., Karakas, A., et al. 2014, ApJ, 791, 14

Neves, V., Santos, N., Sousa, S., Correia, A., & Israelian, G. 2009, A&A, 497, 563

Ramírez, I., Khanal, S., Aleo, P., et al. 2015, ApJ, 808, 13

Ramírez, I., Meléndez, J., Cornejo, D., Roederer, I., & Fish, J. 2011, ApJ, 740, 76

Ramírez, I., Prieto, C., & Lambert, D. 2007, A&A, 465, 271

Reddy, B., Tomkin, J., Lambert, D., & Prieto, C. 2003, MNRAS, 340, 304

Schuler, S., Cunha, K., Smith, V., et al. 2011, ApJ, 737, L32

Scott, P., Asplund, M., Grevesse, N., Bergemann, M., & Sauval, A. 2015a, A&A, 573, A26

Scott, P., Grevesse, N., Asplund, M., et al. 2015b, A&A, 573, A25

Siess, L., Dufour, E., & Forestini, M. 2000, A&A, 358, 593

Sneden, C. 1973, ApJ, 184, 839

Sousa, S., Santos, N., Israelian, G., Mayor, M., & Udry, S. 2011, A&A, 533, A141

Takeda, G., Ford, E., Sills, A., et al. 2007, ApJS, 168, 297

Teske, J., Khanal, S., & Ramírez, I. 2016a, ApJ, 819, 19

Teske, J., Shectman, S., Vogt, S., et al. 2016b, AJ, 152, 167

Tinney, C., Butler, R., Marcy, G., et al. 2005, ApJ, 623, 1171

Tucci Maia, M., Meléndez, J., & Ramírez, I. 2014, ApJ, 790, L25

Valenti, J. & Fischer, D. 2005, ApJS, 159, 141

Wang, J. & Fischer, D. 2014, AJ, 149, 14

Wuchterl, G. & Tscharnuter, W. 2003, A&A, 398, 1081

Yi, S., Demarque, P., Kim, Y., et al. 2001, ApJS, 136, 417

Appendices

Appendix A

Line lists

Table A.1: The line list for the Sun and its solar twin HIP 79672. The columns are from left to right: wavelength, species, EP=excitation potential, g=statistical weight of atomic level, f=oscillator strength of atomic level, EW_=measured equivalent width of the spectra from Hebe, Juno and HIP 79672.

Wavelength[Å]	species	EP	$\log gf$	EW_Hebe	EW_Juno	EW_HIP79672
5052,167	6,0	7,68	-1,30	33,1	35,3	33,1
6587,610	6,0	8,54	-1,02	15,6	14,4	15,6
7113,179	6,0	8,65	-0,76	25,6	24,1	24,9
7116,960	6,0	8,65	-0,91	19,7	19,8	18,4
7771,944	8,0	9,15	0,35	69,0	70,2	72,7
7774,161	8,0	9,15	0,22	61,4	62,7	66,7
7775,390	8,0	9,15	0,00	49,1	52,7	53,8
5682,640	11,0	2,10	-0,77	110,0	108,5	110,9
5688,210	11,0	2,10	-0,48	122,4	123,5	123,7
6154,225	11,0	2,10	-1,55	40,2	39,2	39,6
6160,747	11,0	2,10	-1,25	57,7	57,9	57,7
5711,088	12,0	4,34	-1,73	107,6	106,1	108,0
6318,717	12,0	5,11	-1,95	47,5	49,4	50,0
5557,070	13,0	3,14	-2,21	11,9	12,4	12,7
6696,018	13,0	3,14	-1,48	39,6	38,3	40,7
6698,667	13,0	3,14	-1,78	23,1	23,0	22,3
5517,540	14,0	5,08	-2,50	14,1	14,4	15,8
5645,613	14,0	4,93	-2,04	36,6	37,8	39,5
5665,554	14,0	4,92	-1,94	48,9	42,6	44,6
5684,484	14,0	4,95	-1,55	60,3	61,8	64,7
5690,425	14,0	4,93	-1,77	50,0	51,4	53,2
5701,105	14,0	4,93	-1,95	38,4	42,3	43,0
5753,640	14,0	5,62	-1,33	52,0	49,8	54,1
5948,540	14,0	5,08	-1,21	89,7	84,0	90,4
6125,030	14,0	5,61	-1,51	33,4	33,1	35,4

Table A.1: *Continued from previous page*

Wavelength [Å]	species	EP	log gf	EW_Hebe	EW_Juno	EW_HIP79672
6142,490	14,0	5,62	-1,54	35,8	35,0	37,6
6145,020	14,0	5,61	-1,48	39,2	40,5	41,9
6237,330	14,0	5,61	-1,12	63,9	60,9	62,2
6243,820	14,0	5,62	-1,31	48,2	48,8	52,2
6244,480	14,0	5,61	-1,36	44,0	45,5	49,1
6527,210	14,0	5,87	-1,23	43,4	42,1	46,2
6721,840	14,0	5,86	-1,06	47,5	47,0	50,5
6741,640	14,0	5,98	-1,65	17,3	19,0	18,9
7405,770	14,0	5,61	-0,72	94,3	93,7	95,4
7415,960	14,0	5,61	-0,85	93,6	90,9	95,9
7423,520	14,0	5,62	-0,65	100,8	97,5	104,4
6046,000	16,0	7,87	-0,10	18,2	17,2	19,0
6052,656	16,0	7,87	-0,40	9,9	11,5	11,5
6743,540	16,0	7,87	-0,60	9,5	9,9	9,8
6757,171	16,0	7,87	-0,35	17,3	19,0	18,5
7698,974	19,0	0,00	-0,18	159,2	159,1	158,0
5260,387	20,0	2,52	-1,72	34,5	33,5	35,4
5261,710	20,0	2,52	-0,68	103,1	101,0	103,7
5512,980	20,0	2,93	-0,56	91,1	90,7	93,8
5581,970	20,0	2,52	-0,63	96,1	99,0	101,2
5590,120	20,0	2,52	-0,65	90,7	95,3	98,1
5867,562	20,0	2,93	-1,57	24,4	24,8	25,9
6161,297	20,0	2,52	-1,27	66,6	65,9	68,8
6163,755	20,0	2,52	-1,29	59,3	59,0	60,8
6166,439	20,0	2,52	-1,14	69,8	72,5	73,9
6169,042	20,0	2,52	-0,80	92,8	94,0	100,0
6169,550	20,0	2,52	-0,58	112,5	113,5	113,8
6455,598	20,0	2,52	-1,34	57,4	58,1	60,0
6471,662	20,0	2,53	-0,69	91,4	92,9	98,0
6499,650	20,0	2,52	-0,82	86,1	87,9	89,4
6572,800	20,0	0,00	-4,28	34,2	35,8	36,7
5526,820	21,1	1,77	0,14	75,7	77,9	80,7
5657,880	21,1	1,51	-0,33	68,1	70,2	72,2
5667,140	21,1	1,50	-1,02	34,9	36,2	38,0
5669,055	21,1	1,50	-1,20	38,7	38,8	41,3
5684,214	21,1	1,51	-1,07	37,4	37,9	39,8
6245,641	21,1	1,51	-1,04	35,5	36,3	36,8
6604,578	21,1	1,36	-1,31	34,7	37,3	39,0
4820,410	22,0	1,50	-0,39	44,4	44,3	45,4
4840,880	22,0	0,90	-0,45	65,0	66,4	67,7
4913,616	22,0	1,87	0,22	51,5	51,3	54,3
4964,715	22,0	1,97	-0,82	10,2	9,4	11,0

Table A.1: *Continued from previous page*

Wavelength [Å]	species	EP	log gf	EW_Hebe	EW_Juno	EW_HIP79672
4999,500	22,0	0,83	0,27	107,2	106,1	107,4
5022,866	22,0	0,83	-0,38	75,5	75,5	77,3
5024,850	22,0	0,82	-0,56	70,2	70,5	72,3
5039,960	22,0	0,02	-1,20	78,2	77,8	77,7
5071,490	22,0	1,46	-0,80	32,2	32,7	34,5
5113,439	22,0	1,44	-0,73	27,0	26,7	27,6
5145,459	22,0	1,46	-0,52	36,3	36,3	36,4
5210,380	22,0	0,05	-0,85	91,7	92,9	92,7
5219,699	22,0	0,02	-2,24	28,7	29,7	29,9
5426,260	22,0	0,02	-2,95	7,2	7,4	7,2
5490,147	22,0	1,46	-0,88	21,4	22,0	22,8
5648,570	22,0	2,49	-0,41	11,1	11,0	12,3
5689,459	22,0	2,30	-0,36	12,8	13,4	14,6
5716,441	22,0	2,30	-0,72	6,0	7,5	7,9
5766,330	22,0	3,29	0,33	10,4	11,9	12,8
5866,452	22,0	1,07	-0,84	47,9	48,4	48,8
5953,170	22,0	1,89	-0,27	37,9	36,5	37,1
5965,840	22,0	1,88	-0,49	28,9	27,0	30,5
5978,550	22,0	1,87	-0,60	23,1	23,4	24,4
6126,217	22,0	1,07	-1,42	23,1	23,2	23,2
6258,099	22,0	1,44	-0,30	51,7	53,2	53,6
6261,101	22,0	1,43	-0,48	49,9	49,6	50,7
6599,104	22,0	0,90	-2,03	10,1	11,3	11,1
6743,130	22,0	0,90	-1,63	18,5	19,0	19,8
4865,611	22,1	1,12	-2,81	40,4	40,3	42,3
4874,014	22,1	3,10	-0,80	37,6	38,2	40,0
4911,200	22,1	3,12	-0,61	54,5	52,3	54,0
5005,160	22,1	1,57	-2,72	25,8	26,0	27,4
5154,080	22,1	1,57	-1,75	73,5	75,9	78,7
5185,910	22,1	1,89	-1,49	65,3	64,9	66,6
5211,530	22,1	2,59	-1,16	32,5	33,9	35,4
5418,767	22,1	1,58	-2,11	51,3	49,9	52,6
5490,690	22,1	1,57	-2,43	21,9	21,4	22,6
6606,979	22,1	2,06	-2,76	10,4	9,5	12,1
4875,462	23,0	0,04	-0,81	47,7	47,9	47,5
4881,499	23,0	0,07	-0,66	57,3	60,4	59,7
5670,832	23,0	1,08	-0,42	19,6	20,9	20,8
5703,555	23,0	1,05	-0,21	30,5	33,4	33,3
5727,027	23,0	1,08	-0,01	38,8	40,8	40,4
5727,619	23,0	1,05	-0,88	9,5	10,2	11,4
6039,727	23,0	1,06	-0,65	14,3	13,1	13,9
6081,417	23,0	1,05	-0,58	15,3	15,1	15,3

Table A.1: *Continued from previous page*

Wavelength [Å]	species	EP	log gf	EW_Hebe	EW_Juno	EW_HIP79672
6111,650	23,0	1,04	-0,71	11,6	11,3	11,9
6119,510	23,0	1,06	-0,32	22,2	21,4	22,0
6251,771	23,0	0,29	-1,34	14,9	15,8	15,6
6274,607	23,0	0,27	-1,67	8,7	9,2	9,3
6285,098	23,0	0,28	-1,51	11,1	10,8	10,6
4936,336	24,0	3,11	-0,24	48,6	45,1	47,1
5214,140	24,0	3,37	-0,78	16,7	18,0	18,5
5238,960	24,0	2,71	-1,43	17,2	18,0	18,4
5247,570	24,0	0,96	-1,62	82,2	82,9	84,4
5272,008	24,0	3,45	-0,42	22,6	24,3	27,2
5628,621	24,0	3,42	-0,76	16,6	16,2	17,6
6330,100	24,0	0,94	-2,90	27,3	30,0	29,4
4848,236	24,1	3,86	-1,16	59,3	60,2	62,4
5237,328	24,1	4,07	-1,09	52,5	53,8	55,8
5502,068	24,1	4,17	-2,05	20,3	20,1	22,0
5004,887	25,0	2,92	-1,63	14,8	14,7	14,8
5399,450	25,0	3,85	-0,10	40,8	41,2	42,7
6013,520	25,0	3,07	-0,25	86,3	86,2	87,3
6016,613	25,0	3,07	-0,08	95,4	95,5	96,0
6021,746	25,0	3,08	0,03	97,4	96,6	97,3
4808,150	26,0	3,25	-2,69	26,7	27,3	29,1
4924,770	26,0	2,28	-2,17	101,4	102,3	104,1
4939,680	26,0	0,86	-3,32	95,6	95,2	95,9
4950,100	26,0	3,42	-1,56	77,7	78,6	80,2
4961,910	26,0	3,63	-2,19	26,9	28,0	29,4
4962,570	26,0	4,18	-1,18	54,3	55,3	57,0
4973,090	26,0	3,96	-0,77	92,7	91,6	93,3
5016,480	26,0	4,26	-1,37	31,8	34,2	35,3
5044,211	26,0	2,85	-2,06	70,1	71,8	72,2
5054,640	26,0	3,64	-1,98	41,4	40,9	41,0
5067,140	26,0	4,22	-0,86	66,8	68,6	71,4
5090,770	26,0	4,26	-0,49	92,1	93,5	92,8
5109,650	26,0	4,30	-0,73	73,3	72,8	76,3
5126,190	26,0	4,26	-0,85	63,4	65,5	64,8
5127,360	26,0	0,91	-3,33	95,5	95,6	95,6
5131,470	26,0	2,22	-2,46	92,8	87,1	86,2
5141,740	26,0	2,42	-2,23	90,9	87,1	86,8
5145,090	26,0	2,20	-3,08	57,5	53,1	53,3
5159,050	26,0	4,28	-0,81	68,2	69,3	70,9
5187,910	26,0	4,14	-1,26	56,1	59,5	60,6
5197,940	26,0	4,30	-1,54	37,8	36,5	38,9
5198,710	26,0	2,22	-2,14	98,4	98,0	99,6

Table A.1: *Continued from previous page*

Wavelength [Å]	species	EP	log gf	EW_Hebe	EW_Juno	EW_HIP79672
5217,920	26,0	3,64	-1,72	51,6	50,2	52,0
5225,525	26,0	0,11	-4,78	74,0	74,6	74,5
5228,380	26,0	4,22	-1,19	62,6	61,5	63,7
5242,490	26,0	3,63	-0,99	86,6	86,6	88,4
5243,770	26,0	4,26	-0,99	62,4	62,2	64,1
5247,050	26,0	0,09	-4,96	65,6	66,8	67,6
5250,208	26,0	0,12	-4,94	66,7	67,1	68,1
5250,640	26,0	2,20	-2,09	100,5	102,0	103,9
5253,460	26,0	3,28	-1,57	78,1	77,8	79,2
5398,280	26,0	4,45	-0,63	79,1	74,6	75,6
5409,130	26,0	4,37	-1,06	51,6	53,9	55,8
5432,950	26,0	4,45	-0,94	73,1	74,2	77,2
5441,340	26,0	4,31	-1,63	32,3	34,1	34,9
5461,550	26,0	4,45	-1,80	26,7	26,1	27,9
5464,280	26,0	4,14	-1,58	38,5	38,5	40,0
5470,090	26,0	4,45	-1,71	27,2	27,1	27,8
5472,710	26,0	4,21	-1,52	44,4	44,6	45,7
5473,900	26,0	4,15	-0,72	82,3	82,6	84,9
5483,100	26,0	4,15	-1,45	43,8	43,7	45,4
5487,150	26,0	4,42	-1,43	39,1	38,9	40,2
5491,832	26,0	4,19	-2,19	15,2	14,2	13,9
5501,470	26,0	0,96	-3,06	119,3	118,4	119,3
5522,450	26,0	4,21	-1,45	42,9	44,1	45,8
5525,540	26,0	4,23	-1,12	56,7	56,9	57,9
5543,940	26,0	4,22	-1,04	64,4	63,8	65,3
5546,510	26,0	4,37	-1,21	52,2	53,1	54,4
5554,890	26,0	4,55	-0,36	97,9	101,3	102,8
5560,210	26,0	4,43	-1,09	52,4	54,3	55,9
5576,090	26,0	3,43	-0,94	118,0	118,1	119,3
5577,020	26,0	5,03	-1,54	11,8	12,9	14,7
5584,760	26,0	3,57	-2,22	39,9	42,9	43,1
5600,224	26,0	4,26	-1,42	39,4	42,7	45,8
5618,630	26,0	4,21	-1,27	53,5	52,7	54,3
5619,600	26,0	4,39	-1,60	37,5	36,7	37,2
5633,950	26,0	4,99	-0,23	64,3	66,6	68,2
5635,820	26,0	4,26	-1,79	31,9	35,3	36,3
5636,700	26,0	3,64	-2,51	18,9	21,1	22,4
5638,260	26,0	4,22	-0,77	77,6	78,5	80,6
5650,710	26,0	5,09	-0,86	41,3	41,0	43,0
5651,469	26,0	4,47	-1,75	18,1	20,7	21,3
5653,870	26,0	4,39	-1,54	39,4	40,4	43,5
5661,348	26,0	4,28	-1,76	20,6	24,6	25,6

Table A.1: *Continued from previous page*

Wavelength [Å]	species	EP	log gf	EW_Hebe	EW_Juno	EW_HIP79672
5679,023	26,0	4,65	-0,75	60,2	61,6	63,7
5686,530	26,0	4,55	-0,57	82,4	79,8	82,4
5696,090	26,0	4,55	-1,72	13,7	15,4	16,0
5701,544	26,0	2,56	-2,16	86,5	88,4	89,8
5705,464	26,0	4,30	-1,36	39,9	41,0	42,9
5717,830	26,0	4,28	-1,03	56,7	60,3	61,7
5731,760	26,0	4,26	-1,20	57,7	58,6	60,2
5741,850	26,0	4,26	-1,67	30,2	33,4	34,9
5752,030	26,0	4,55	-1,18	54,3	55,8	57,1
5852,220	26,0	4,55	-1,23	41,8	41,4	42,0
5856,090	26,0	4,29	-1,46	35,9	35,2	36,1
5858,780	26,0	4,22	-2,16	13,3	13,6	14,0
5859,590	26,0	4,55	-0,58	75,0	75,6	76,1
5861,110	26,0	4,28	-2,30	10,7	11,4	9,9
5862,360	26,0	4,55	-0,13	88,8	88,8	90,1
5902,470	26,0	4,59	-1,71	12,7	12,8	12,0
5905,670	26,0	4,65	-0,69	59,7	59,0	60,1
5909,970	26,0	3,21	-2,60	33,0	33,0	37,5
5916,250	26,0	2,45	-2,99	48,5	50,0	50,5
5927,790	26,0	4,65	-0,99	42,7	43,2	45,4
5929,680	26,0	4,55	-1,31	40,5	40,6	44,1
5930,180	26,0	4,65	-0,17	89,1	90,4	92,5
5934,650	26,0	3,93	-1,07	76,8	76,9	78,7
5952,720	26,0	3,98	-1,34	63,9	62,9	64,7
5976,780	26,0	3,94	-1,24	68,7	69,1	71,1
6003,010	26,0	3,88	-1,06	85,2	83,9	85,4
6024,060	26,0	4,55	-0,02	112,0	107,8	110,4
6054,070	26,0	4,37	-2,33	5,7	7,7	7,8
6056,000	26,0	4,73	-0,40	73,8	74,9	76,7
6065,482	26,0	2,61	-1,53	115,0	116,8	116,6
6078,490	26,0	4,80	-0,32	73,0	73,8	74,6
6079,010	26,0	4,65	-1,02	39,8	41,0	42,0
6082,710	26,0	2,22	-3,57	33,5	34,1	34,9
6085,260	26,0	2,76	-3,05	41,1	40,6	42,1
6093,644	26,0	4,61	-1,30	30,5	31,1	31,5
6096,665	26,0	3,98	-1,81	36,4	37,8	39,2
6127,910	26,0	4,14	-1,40	51,9	48,2	49,3
6151,618	26,0	2,18	-3,28	47,2	50,0	49,4
6157,720	26,0	4,07	-1,20	60,5	61,4	62,7
6165,360	26,0	4,14	-1,46	42,8	45,2	46,2
6170,510	26,0	4,80	-0,38	84,3	85,4	86,8
6173,335	26,0	2,22	-2,88	70,8	69,9	70,4

Table A.1: *Continued from previous page*

Wavelength [Å]	species	EP	log gf	EW_Hebe	EW_Juno	EW_HIP79672
6180,200	26,0	2,73	-2,63	57,5	56,6	57,5
6187,990	26,0	3,94	-1,62	47,3	48,4	50,1
6213,430	26,0	2,22	-2,52	80,8	83,2	83,8
6219,280	26,0	2,20	-2,43	89,0	90,0	90,8
6229,230	26,0	2,85	-2,83	39,7	38,7	39,6
6232,640	26,0	3,65	-1,22	88,5	85,2	87,9
6240,646	26,0	2,22	-3,29	51,9	47,6	45,2
6265,134	26,0	2,18	-2,55	84,5	84,9	86,5
6311,500	26,0	2,83	-3,14	32,1	29,6	30,2
6322,690	26,0	2,59	-2,43	77,2	78,0	82,1
6335,330	26,0	2,20	-2,26	98,5	100,8	101,4
6336,820	26,0	3,69	-0,93	108,2	108,1	110,7
6344,150	26,0	2,43	-2,92	64,1	61,7	63,8
6355,030	26,0	2,84	-2,31	74,0	75,3	78,3
6380,740	26,0	4,19	-1,32	50,3	53,0	52,0
6430,846	26,0	2,18	-2,01	113,7	115,0	113,6
6481,870	26,0	2,28	-2,98	61,9	64,3	64,0
6498,939	26,0	0,96	-4,70	44,5	47,0	46,9
6518,367	26,0	2,83	-2,45	58,3	59,9	62,0
6574,229	26,0	0,99	-5,01	33,4	34,1	35,6
6593,871	26,0	2,43	-2,39	87,0	86,2	87,1
6597,560	26,0	4,80	-0,97	44,2	45,5	47,1
6609,110	26,0	2,56	-2,68	64,5	66,7	67,8
6699,142	26,0	4,59	-2,10	8,9	10,0	9,3
6703,567	26,0	2,76	-3,02	37,3	38,3	38,7
6705,102	26,0	4,61	-0,98	44,6	46,5	47,3
6713,745	26,0	4,80	-1,40	20,3	22,0	22,6
6726,667	26,0	4,61	-1,03	46,9	46,7	48,6
6739,522	26,0	1,56	-4,79	10,9	11,9	12,3
6750,152	26,0	2,42	-2,62	73,6	75,0	75,3
6752,710	26,0	4,64	-1,22	36,4	36,9	38,6
6810,263	26,0	4,61	-0,99	50,0	49,9	52,0
6828,590	26,0	4,64	-0,82	53,4	55,7	56,5
6837,006	26,0	4,59	-1,69	17,6	20,4	21,9
6841,340	26,0	4,61	-0,71	67,0	66,4	71,3
6842,690	26,0	4,64	-1,22	38,5	42,6	44,1
6843,660	26,0	4,55	-0,83	58,9	64,6	65,5
6854,823	26,0	4,59	-1,93	13,3	14,0	13,7
6855,160	26,0	4,56	-0,74	73,9	73,0	74,4
6858,150	26,0	4,61	-0,94	51,3	53,2	55,1
7090,380	26,0	4,23	-1,11	64,3	65,9	68,3
7132,990	26,0	4,08	-1,65	40,9	43,9	44,7

Table A.1: *Continued from previous page*

Wavelength [Å]	species	EP	log gf	EW_Hebe	EW_Juno	EW_HIP79672
7401,685	26,0	4,19	-1,50	42,1	41,4	43,9
7418,670	26,0	4,14	-1,38	49,3	49,9	50,3
7583,790	26,0	3,02	-1,88	84,9	86,1	86,3
7710,360	26,0	4,22	-1,11	67,8	71,9	70,0
7723,210	26,0	2,28	-3,62	40,6	40,3	40,6
4993,340	26,1	2,81	-3,73	38,9	39,7	41,0
5132,660	26,1	2,81	-4,17	23,8	23,9	24,2
5197,577	26,1	3,23	-2,22	81,4	80,7	83,9
5234,624	26,1	3,22	-2,18	84,4	86,3	89,1
5264,804	26,1	3,23	-3,13	46,5	48,0	50,0
5414,072	26,1	3,22	-3,58	26,4	27,8	30,1
5425,257	26,1	3,20	-3,22	39,6	42,5	43,8
5534,840	26,1	3,24	-2,88	60,9	58,3	59,9
6084,090	26,1	3,20	-3,83	20,5	20,4	21,7
6149,240	26,1	3,89	-2,75	36,1	35,5	36,9
6238,380	26,1	3,89	-2,63	45,8	46,4	44,2
6369,462	26,1	2,89	-4,11	20,4	19,6	21,2
6432,676	26,1	2,89	-3,57	43,7	43,3	46,4
6516,077	26,1	2,89	-3,31	60,1	55,8	60,2
7224,479	26,1	3,89	-3,20	23,3	22,6	22,9
7711,721	26,1	3,90	-2,50	49,3	52,1	51,7
4813,478	27,0	3,22	0,18	48,7	47,4	47,9
5530,776	27,0	1,71	-2,23	18,6	19,1	19,0
5647,232	27,0	2,28	-1,56	14,1	15,3	15,5
6082,421	27,0	3,51	-0,52	14,2	13,8	14,3
6454,946	27,0	3,63	-0,25	14,7	16,0	15,1
7417,385	27,0	2,04	-2,07	11,2	11,1	12,3
4831,180	28,0	3,61	-0,32	73,5	73,9	75,3
4866,270	28,0	3,54	-0,21	77,5	76,5	77,9
4904,420	28,0	3,54	-0,25	88,1	87,9	89,8
4913,980	28,0	3,74	-0,66	56,6	56,6	58,8
4946,040	28,0	3,80	-1,22	28,1	26,9	29,8
4952,290	28,0	3,61	-1,26	32,2	32,7	34,2
4953,210	28,0	3,74	-0,58	56,5	57,8	58,2
4976,135	28,0	3,61	-1,25	31,6	30,0	31,0
4998,220	28,0	3,61	-0,69	57,2	56,1	56,8
5010,940	28,0	3,63	-0,90	49,6	50,1	51,1
5082,350	28,0	3,66	-0,59	70,1	68,0	69,0
5084,110	28,0	3,68	-0,06	93,3	94,3	94,9
5094,420	28,0	3,83	-1,07	31,5	32,9	32,2
5102,970	28,0	1,68	-2,66	50,8	50,2	50,4
5157,980	28,0	3,61	-1,51	20,6	19,5	21,0

Table A.1: *Continued from previous page*

Wavelength [Å]	species	EP	log gf	EW_Hebe	EW_Juno	EW_HIP79672
5578,729	28,0	1,68	-2,57	59,2	59,7	59,9
5587,870	28,0	1,93	-2,44	57,6	56,9	64,1
5589,360	28,0	3,90	-1,15	27,8	28,8	30,2
5593,746	28,0	3,90	-0,78	43,3	45,6	46,8
5625,320	28,0	4,09	-0,73	40,0	39,3	40,9
5628,350	28,0	4,09	-1,32	16,4	15,5	16,6
5638,750	28,0	3,90	-1,70	10,5	10,7	11,7
5641,880	28,0	4,11	-1,02	30,3	27,2	28,4
5643,080	28,0	4,16	-1,23	17,7	17,4	18,2
5694,990	28,0	4,09	-0,63	43,9	44,9	45,5
5748,360	28,0	1,68	-3,24	29,1	28,9	29,5
5754,670	28,0	1,93	-1,85	80,3	78,3	78,2
5996,740	28,0	4,24	-1,01	21,8	21,9	22,4
6007,317	28,0	1,68	-3,41	26,9	27,5	27,5
6086,288	28,0	4,27	-0,46	43,5	42,7	44,8
6108,120	28,0	1,68	-2,43	67,5	66,6	67,8
6111,080	28,0	4,09	-0,81	36,1	35,5	36,4
6119,760	28,0	4,27	-1,32	10,7	11,0	11,1
6130,140	28,0	4,27	-0,94	24,5	22,9	23,4
6175,370	28,0	4,09	-0,55	52,4	53,1	52,8
6176,798	28,0	4,09	-0,26	65,0	64,5	65,2
6177,250	28,0	1,83	-3,51	16,3	16,2	15,6
6186,717	28,0	4,11	-0,88	29,7	32,0	32,4
6204,605	28,0	4,09	-1,10	21,9	22,6	22,9
6223,991	28,0	4,11	-1,05	28,8	28,2	30,1
6230,100	28,0	4,11	-1,13	24,3	22,6	24,1
6322,169	28,0	4,15	-1,21	19,3	20,2	21,8
6327,600	28,0	1,68	-3,06	38,8	38,9	40,0
6360,810	28,0	4,17	-1,15	18,3	17,4	19,3
6378,258	28,0	4,15	-0,97	33,1	33,4	33,4
6482,810	28,0	1,93	-2,76	45,9	42,1	45,8
6598,611	28,0	4,24	-0,91	25,5	25,4	27,2
6635,130	28,0	4,42	-0,72	25,7	25,3	28,2
6643,640	28,0	1,68	-2,03	95,5	96,0	95,6
6767,780	28,0	1,83	-2,10	81,4	82,7	82,8
6772,320	28,0	3,66	-0,97	50,3	52,7	53,0
6842,043	28,0	3,66	-1,50	27,9	28,9	27,7
7110,900	28,0	1,94	-2,88	39,5	38,9	38,3
7715,591	28,0	3,70	-1,01	53,3	51,6	55,1
7748,890	28,0	3,70	-0,38	90,4	89,4	90,1
5105,558	29,0	1,39	-1,52	87,0	84,0	84,9
5218,202	29,0	3,82	0,48	51,4	51,7	52,9

Table A.1: *Continued from previous page*

Wavelength [Å]	species	EP	log gf	EW_Hebe	EW_Juno	EW_HIP79672
7933,131	29,0	3,79	-0,37	33,2	31,8	32,6
4810,534	30,0	4,08	-0,16	74,4	74,3	74,3
6362,347	30,0	5,80	0,14	22,6	22,4	25,3
4854,867	39,1	0,99	-0,38	50,6	50,8	53,5
4883,685	39,1	1,08	0,07	58,1	58,2	61,2
4900,110	39,1	1,03	-0,09	57,4	56,1	59,6
5087,418	39,1	1,08	-0,17	47,8	48,8	51,3
5119,111	39,1	0,99	-1,36	20,8	20,5	19,4
5200,411	39,1	0,99	-0,57	39,5	38,2	42,5
5853,696	56,1	0,60	-0,91	66,4	64,9	68,6
6141,695	56,1	0,70	-0,08	117,3	116,3	122,7
6496,900	56,1	0,60	-0,38	100,3	100,0	106,5
5274,230	58,1	1,04	0,13	11,0	10,9	12,9
6645,100	63,1	1,38	0,12	5,2	6,0	7,0

Table A.2: The line list of HD 90722 and HD 102117. The columns are from left to right: wavelength, species, EP=excitation potential, g=statistical weight of atomic level, f=oscillator strength of atomic level, EW_=measured equivalent width of the spectra from Hebe, Juno and HIP 79672.

Wavelength [Å]	species	EP	log gf	EW_HD90722	EW_HD102117
5052,167	6,0	7,68	-1,30	47,1	46,7
6587,610	6,0	8,54	-1,02	25,8	22,4
7113,179	6,0	8,65	-0,76	43,3	36,4
7116,960	6,0	8,65	-0,91	42,8	37,1
7771,944	8,0	9,15	0,35	83,5	79,6
7774,161	8,0	9,15	0,22	84,1	72,5
7775,390	8,0	9,15	0,00	73,4	67,7
5682,640	11,0	2,10	-0,77	156,6	154,0
5688,210	11,0	2,10	-0,48	170,4	154,7
6154,225	11,0	2,10	-1,55	66,2	66,0
6160,747	11,0	2,10	-1,25	95,2	87,3
5711,088	12,0	4,34	-1,73	132,4	131,1
6318,717	12,0	5,11	-1,95	78,7	78,2
5557,070	13,0	3,14	-2,21	27,2	26,6
6696,018	13,0	3,14	-1,48	65,2	65,4
6698,667	13,0	3,14	-1,78	43,3	42,6
5517,540	14,0	5,08	-2,50	27,2	26,3
5645,613	14,0	4,93	-2,04	61,7	58,8
5665,554	14,0	4,92	-1,94	69,0	63,3
5684,484	14,0	4,95	-1,55	85,0	81,3

Table A.2: *Continued from previous page*

Wavelength [Å]	species	EP	log gf	EW_HD90722	EW_HD102117
5690,425	14,0	4,93	-1,77	71,3	69,0
5701,105	14,0	4,93	-1,95	59,1	56,7
5753,640	14,0	5,62	-1,33	89,3	85,9
5772,145	14,0	5,08	-1,65	76,6	73,2
5793,073	14,0	4,93	-1,96	65,8	64,0
5948,540	14,0	5,08	-1,21	108,1	112,1
6125,030	14,0	5,61	-1,51	58,8	53,2
6142,490	14,0	5,62	-1,54	60,1	54,9
6145,020	14,0	5,61	-1,48	63,9	61,3
6237,330	14,0	5,61	-1,12	101,9	97,5
6243,820	14,0	5,62	-1,31	68,8	70,9
6244,480	14,0	5,61	-1,36	79,2	73,3
6527,210	14,0	5,87	-1,23	71,5	66,9
6721,840	14,0	5,86	-1,06	78,5	69,7
6741,640	14,0	5,98	-1,65	38,2	33,3
7405,770	14,0	5,61	-0,72	123,7	118,9
6046,000	16,0	7,87	-0,10	35,5	30,6
6052,656	16,0	7,87	-0,40	25,2	20,0
6743,540	16,0	7,87	-0,60	16,3	12,2
6757,171	16,0	7,87	-0,35	29,8	25,8
7698,974	19,0	0,00	-0,18	186,3	186,7
5260,387	20,0	2,52	-1,72	53,9	53,9
5512,980	20,0	2,93	-0,56	109,3	112,2
5581,970	20,0	2,52	-0,63	119,8	118,0
5590,120	20,0	2,52	-0,65	107,5	111,0
5867,562	20,0	2,93	-1,57	43,5	43,3
6161,297	20,0	2,52	-1,27	97,7	94,9
6163,755	20,0	2,52	-1,29	77,6	76,5
6166,439	20,0	2,52	-1,14	90,1	90,5
6169,042	20,0	2,52	-0,80	117,0	118,0
6455,598	20,0	2,52	-1,34	81,0	80,0
6471,662	20,0	2,53	-0,69	112,2	117,6
6499,650	20,0	2,52	-0,82	110,8	110,6
6572,800	20,0	0,00	-4,28	60,9	64,8
5657,880	21,1	1,51	-0,33	89,0	85,5
5667,140	21,1	1,50	-1,02	61,5	57,3
5669,055	21,1	1,50	-1,20	64,7	58,9
5684,214	21,1	1,51	-1,07	59,7	55,1
6245,641	21,1	1,51	-1,04	54,0	52,3
6604,578	21,1	1,36	-1,31	58,1	55,3
5022,866	22,0	0,83	-0,38	90,6	93,2
5024,850	22,0	0,82	-0,56	90,5	92,4

Table A.2: *Continued from previous page*

Wavelength [Å]	species	EP	log gf	EW_HD90722	EW_HD102117
5039,960	22,0	0,02	-1,20	102,8	100,5
5071,490	22,0	1,46	-0,80	55,9	56,0
5113,439	22,0	1,44	-0,73	44,2	47,0
5145,459	22,0	1,46	-0,52	59,5	60,4
5210,380	22,0	0,05	-0,85	116,4	117,1
5219,699	22,0	0,02	-2,24	47,1	52,6
5426,260	22,0	0,02	-2,95	15,4	17,6
5490,147	22,0	1,46	-0,88	39,9	38,7
5648,570	22,0	2,49	-0,41	26,0	26,3
5689,459	22,0	2,30	-0,36	29,7	28,6
5716,441	22,0	2,30	-0,72	13,8	13,5
5766,330	22,0	3,29	0,33	21,4	20,8
5866,452	22,0	1,07	-0,84	77,8	76,5
5953,170	22,0	1,89	-0,27	63,1	62,8
5965,840	22,0	1,88	-0,49	58,1	60,0
5978,550	22,0	1,87	-0,60	42,1	42,6
6126,217	22,0	1,07	-1,42	41,0	43,6
6258,099	22,0	1,44	-0,30	70,2	71,3
6261,101	22,0	1,43	-0,48	75,2	76,3
6599,104	22,0	0,90	-2,03	23,4	22,0
6743,130	22,0	0,90	-1,63	38,6	39,8
5154,080	22,1	1,57	-1,75	107,5	104,8
5185,910	22,1	1,89	-1,49	81,0	79,8
5211,530	22,1	2,59	-1,16	45,7	45,8
5418,767	22,1	1,58	-2,11	68,3	65,4
5490,690	22,1	1,57	-2,43	40,4	35,4
6606,979	22,1	2,06	-2,76	16,7	16,0
5670,832	23,0	1,08	-0,42	45,3	43,9
5703,555	23,0	1,05	-0,21	62,2	60,8
5727,027	23,0	1,08	-0,01	72,3	72,3
5727,619	23,0	1,05	-0,88	22,5	22,4
6039,727	23,0	1,06	-0,65	31,8	28,9
6081,417	23,0	1,05	-0,58	37,5	34,6
6111,650	23,0	1,04	-0,71	30,3	32,1
6119,510	23,0	1,06	-0,32	43,3	41,7
6251,771	23,0	0,29	-1,34	36,2	37,2
6274,607	23,0	0,27	-1,67	20,9	22,3
6285,098	23,0	0,28	-1,51	26,9	27,2
5214,140	24,0	3,37	-0,78	31,3	35,9
5238,960	24,0	2,71	-1,43	29,6	31,2
5247,570	24,0	0,96	-1,62	105,1	104,8
5272,008	24,0	3,45	-0,42	40,1	39,8

Table A.2: *Continued from previous page*

Wavelength [Å]	species	EP	log gf	EW_HD90722	EW_HD102117
5628,621	24,0	3,42	-0,76	33,2	33,7
5781,163	24,0	3,01	-1,00	36,8	33,9
5783,073	24,0	3,23	-0,48	75,7	74,7
5783,870	24,0	3,32	-0,29	71,3	70,0
5787,930	24,0	3,32	-0,08	70,5	69,5
6330,100	24,0	0,94	-2,90	47,6	47,2
5237,328	24,1	4,07	-1,09	71,8	71,0
5502,068	24,1	4,17	-2,05	33,3	31,1
5399,450	25,0	3,85	-0,10	71,5	66,2
6013,520	25,0	3,07	-0,25	120,5	117,5
6016,613	25,0	3,07	-0,08	122,6	123,4
6021,746	25,0	3,08	0,03	126,3	121,5
5044,211	26,0	2,85	-2,06	88,2	87,9
5054,640	26,0	3,64	-1,98	60,5	61,2
5067,140	26,0	4,22	-0,86	88,5	88,3
5109,650	26,0	4,30	-0,73	99,6	97,7
5126,190	26,0	4,26	-0,85	99,9	99,7
5141,740	26,0	2,42	-2,23	116,7	109,9
5145,090	26,0	2,20	-3,08	77,5	73,5
5159,050	26,0	4,28	-0,81	92,6	92,0
5187,910	26,0	4,14	-1,26	90,9	88,7
5197,940	26,0	4,30	-1,54	57,9	49,6
5217,920	26,0	3,64	-1,72	73,9	72,7
5225,525	26,0	0,11	-4,79	96,8	99,5
5228,380	26,0	4,22	-1,19	87,6	88,7
5242,490	26,0	3,63	-0,99	105,7	104,1
5243,770	26,0	4,26	-0,99	84,9	81,7
5247,050	26,0	0,09	-4,96	86,4	85,3
5250,208	26,0	0,12	-4,94	96,7	97,2
5253,020	26,0	2,28	-3,84	36,9	35,5
5253,460	26,0	3,28	-1,57	99,4	99,7
5285,130	26,0	4,43	-1,54	51,2	50,0
5288,520	26,0	3,69	-1,51	79,5	80,2
5293,960	26,0	4,14	-1,77	54,6	53,4
5295,310	26,0	4,42	-1,59	50,8	48,2
5307,360	26,0	1,61	-2,97	118,0	116,1
5321,100	26,0	4,43	-1,26	63,1	61,4
5322,040	26,0	2,28	-2,89	80,9	81,0
5365,400	26,0	3,57	-1,25	93,9	91,7
5373,710	26,0	4,47	-0,74	77,9	77,9
5379,570	26,0	3,69	-1,51	82,8	80,1
5386,330	26,0	4,15	-1,67	50,1	50,3

Table A.2: *Continued from previous page*

Wavelength [Å]	species	EP	log gf	EW_HD90722	EW_HD102117
5389,480	26,0	4,41	-0,45	104,9	103,5
5398,280	26,0	4,45	-0,63	92,0	91,2
5409,130	26,0	4,37	-1,06	88,5	83,0
5432,950	26,0	4,45	-0,94	90,8	88,8
5441,340	26,0	4,31	-1,63	58,5	57,1
5461,550	26,0	4,45	-1,80	46,7	42,7
5464,280	26,0	4,14	-1,58	53,7	51,4
5470,090	26,0	4,45	-1,71	50,0	48,9
5472,710	26,0	4,21	-1,52	67,4	66,7
5473,900	26,0	4,15	-0,72	108,7	109,1
5483,100	26,0	4,15	-1,45	72,0	71,7
5487,150	26,0	4,42	-1,43	67,1	61,7
5491,832	26,0	4,19	-2,19	32,0	27,6
5522,450	26,0	4,21	-1,45	62,1	62,3
5525,540	26,0	4,23	-1,12	80,3	80,1
5543,940	26,0	4,22	-1,04	85,4	83,5
5546,510	26,0	4,37	-1,21	70,3	68,3
5560,210	26,0	4,43	-1,09	70,0	69,8
5577,020	26,0	5,03	-1,54	25,2	23,2
5600,224	26,0	4,26	-1,42	59,7	60,1
5618,630	26,0	4,21	-1,27	70,3	68,8
5619,600	26,0	4,39	-1,60	60,1	60,3
5633,950	26,0	4,99	-0,23	95,5	90,6
5635,820	26,0	4,26	-1,79	53,7	52,9
5636,700	26,0	3,64	-2,51	35,9	35,9
5638,260	26,0	4,22	-0,77	98,3	97,4
5650,710	26,0	5,09	-0,86	68,3	65,3
5651,469	26,0	4,47	-1,75	37,7	35,6
5653,870	26,0	4,39	-1,54	65,7	64,0
5661,348	26,0	4,28	-1,76	44,1	42,9
5679,023	26,0	4,65	-0,75	81,3	79,2
5701,544	26,0	2,56	-2,16	109,5	106,8
5705,464	26,0	4,30	-1,36	56,6	55,7
5717,830	26,0	4,28	-1,03	86,7	86,7
5731,760	26,0	4,26	-1,20	76,3	77,7
5741,850	26,0	4,26	-1,67	50,8	50,6
5752,030	26,0	4,55	-1,18	76,1	74,1
5775,080	26,0	4,22	-1,30	77,4	77,5
5778,453	26,0	2,59	-3,44	37,8	39,5
5784,658	26,0	3,40	-2,53	49,2	47,7
5793,914	26,0	4,22	-1,62	59,1	54,9
5806,730	26,0	4,61	-0,95	75,9	75,8

Table A.2: *Continued from previous page*

Wavelength [Å]	species	EP	log gf	EW_HD90722	EW_HD102117
5809,218	26,0	3,88	-1,71	76,4	76,3
5814,810	26,0	4,28	-1,87	40,6	39,7
5837,700	26,0	4,29	-2,24	20,9	23,4
5849,680	26,0	3,69	-2,89	17,8	16,8
5852,220	26,0	4,55	-1,23	63,2	63,2
5856,090	26,0	4,29	-1,46	53,3	52,5
5858,780	26,0	4,22	-2,16	25,8	24,9
5859,590	26,0	4,55	-0,58	96,4	94,3
5861,110	26,0	4,28	-2,30	19,2	19,6
5862,360	26,0	4,55	-0,12	111,4	111,1
5905,670	26,0	4,65	-0,69	83,1	77,8
5909,970	26,0	3,21	-2,60	60,9	59,8
5916,250	26,0	2,45	-2,99	80,0	73,6
5927,790	26,0	4,65	-0,99	67,9	63,4
5929,680	26,0	4,55	-1,31	63,7	63,1
5930,180	26,0	4,65	-0,17	115,8	115,9
5934,650	26,0	3,93	-1,07	105,9	105,1
5952,720	26,0	3,98	-1,34	91,4	88,4
5976,780	26,0	3,94	-1,24	94,5	94,5
6003,010	26,0	3,88	-1,06	103,1	104,9
6056,000	26,0	4,73	-0,40	98,3	97,1
6078,490	26,0	4,80	-0,32	105,9	105,1
6079,010	26,0	4,65	-1,02	69,6	69,6
6082,710	26,0	2,22	-3,57	65,6	65,9
6093,644	26,0	4,61	-1,30	56,4	56,3
6096,665	26,0	3,98	-1,81	61,4	60,6
6127,910	26,0	4,14	-1,40	70,9	68,7
6151,618	26,0	2,18	-3,28	73,2	71,4
6157,720	26,0	4,07	-1,20	82,1	87,2
6165,360	26,0	4,14	-1,46	64,5	61,7
6170,510	26,0	4,80	-0,38	119,4	119,4
6173,335	26,0	2,22	-2,88	90,6	90,3
6180,200	26,0	2,73	-2,63	85,7	85,7
6187,990	26,0	3,94	-1,62	70,6	68,9
6200,313	26,0	2,60	-2,41	101,7	101,3
6213,430	26,0	2,22	-2,52	103,1	101,3
6219,280	26,0	2,20	-2,43	117,9	115,5
6229,230	26,0	2,85	-2,83	62,1	58,6
6232,640	26,0	3,65	-1,22	110,6	108,4
6240,646	26,0	2,22	-3,29	72,9	72,7
6265,134	26,0	2,18	-2,55	111,2	107,0
6297,793	26,0	2,22	-2,72	96,4	98,4

Table A.2: *Continued from previous page*

Wavelength [Å]	species	EP	log gf	EW_HD90722	EW_HD102117
6311,500	26,0	2,83	-3,14	54,2	51,8
6322,690	26,0	2,59	-2,43	104,5	101,2
6344,150	26,0	2,43	-2,92	84,5	85,1
6380,740	26,0	4,19	-1,32	75,6	75,3
6419,950	26,0	4,73	-0,24	111,4	109,7
6481,870	26,0	2,28	-2,98	94,2	87,2
6498,939	26,0	0,96	-4,70	72,3	71,1
6518,367	26,0	2,83	-2,45	81,9	84,3
6574,229	26,0	0,99	-5,01	51,0	50,5
6593,871	26,0	2,43	-2,39	108,2	107,2
6597,560	26,0	4,80	-0,97	62,1	61,5
6609,110	26,0	2,56	-2,68	95,5	93,9
6699,142	26,0	4,59	-2,10	17,0	16,1
6703,567	26,0	2,76	-3,02	63,6	63,6
6705,102	26,0	4,61	-0,98	73,8	73,1
6713,745	26,0	4,80	-1,40	41,4	39,9
6726,667	26,0	4,61	-1,03	66,5	64,6
6739,522	26,0	1,56	-4,79	29,2	29,1
6750,152	26,0	2,42	-2,62	95,9	94,7
6752,710	26,0	4,64	-1,22	59,8	59,0
6793,259	26,0	4,07	-2,32	28,1	25,2
6810,263	26,0	4,61	-0,99	74,8	70,3
6828,590	26,0	4,64	-0,82	80,5	75,4
6837,006	26,0	4,59	-1,69	34,3	33,0
6841,340	26,0	4,61	-0,71	92,2	88,7
6842,690	26,0	4,64	-1,22	62,2	57,7
6843,660	26,0	4,55	-0,83	93,9	89,2
6854,823	26,0	4,59	-1,93	33,5	28,3
6855,160	26,0	4,56	-0,74	98,2	93,0
6858,150	26,0	4,61	-0,94	77,2	71,8
6945,205	26,0	2,42	-2,45	113,7	105,7
6978,852	26,0	2,48	-2,47	106,6	108,1
6999,880	26,0	4,10	-1,46	81,7	79,3
7022,950	26,0	4,19	-1,15	84,3	82,5
7038,220	26,0	4,22	-1,20	98,3	87,6
7090,380	26,0	4,23	-1,11	89,2	86,7
7132,990	26,0	4,08	-1,65	64,4	63,5
7401,685	26,0	4,19	-1,50	66,2	66,9
7418,670	26,0	4,14	-1,38	73,1	68,9
7583,790	26,0	3,02	-1,88	118,0	111,0
7710,360	26,0	4,22	-1,11	84,4	83,7
7723,210	26,0	2,28	-3,62	68,3	65,9

Table A.2: *Continued from previous page*

Wavelength [Å]	species	EP	log gf	EW_HD90722	EW_HD102117
5197,577	26,1	3,23	-2,22	92,3	84,2
5234,624	26,1	3,22	-2,18	103,4	100,9
5264,804	26,1	3,23	-3,13	59,5	56,6
5325,550	26,1	3,22	-3,25	54,6	51,9
5414,072	26,1	3,22	-3,58	46,3	40,3
5425,257	26,1	3,20	-3,22	56,0	53,3
5534,840	26,1	3,24	-2,88	80,1	78,3
6084,090	26,1	3,20	-3,83	33,3	29,1
6149,240	26,1	3,89	-2,75	53,1	48,9
6238,380	26,1	3,89	-2,63	65,0	61,7
6369,462	26,1	2,89	-4,11	31,1	29,8
6416,920	26,1	3,89	-2,75	55,7	55,2
6432,676	26,1	2,89	-3,57	59,2	56,2
6516,077	26,1	2,89	-3,31	74,2	69,1
7224,479	26,1	3,89	-3,20	35,7	31,7
7515,831	26,1	3,90	-3,39	19,8	17,9
7711,721	26,1	3,90	-2,50	66,1	59,2
5530,776	27,0	1,71	-2,23	48,0	43,8
5647,232	27,0	2,28	-1,56	36,3	35,1
6082,421	27,0	3,51	-0,52	36,0	31,7
6454,946	27,0	3,63	-0,25	32,6	30,5
7417,385	27,0	2,04	-2,07	28,2	28,6
5082,350	28,0	3,66	-0,59	89,4	87,5
5084,110	28,0	3,68	-0,06	104,3	103,8
5094,420	28,0	3,83	-1,07	52,8	49,1
5102,970	28,0	1,68	-2,66	78,5	76,6
5157,980	28,0	3,61	-1,51	39,5	40,0
5578,729	28,0	1,68	-2,57	83,0	79,9
5587,870	28,0	1,93	-2,44	74,4	73,9
5589,360	28,0	3,90	-1,15	47,7	47,3
5593,746	28,0	3,90	-0,78	66,9	64,3
5625,320	28,0	4,09	-0,73	70,0	68,2
5628,350	28,0	4,09	-1,32	41,9	38,9
5638,750	28,0	3,90	-1,70	23,0	20,5
5641,880	28,0	4,11	-1,02	40,0	42,9
5643,080	28,0	4,16	-1,23	32,4	30,9
5694,990	28,0	4,09	-0,63	63,0	63,0
5748,360	28,0	1,68	-3,24	53,2	51,8
5754,670	28,0	1,93	-1,85	97,1	96,8
5805,220	28,0	4,17	-0,62	63,2	60,4
5847,010	28,0	1,68	-3,41	45,4	44,4
5996,740	28,0	4,24	-1,01	40,2	36,4

Table A.2: *Continued from previous page*

Wavelength [Å]	species	EP	log gf	EW_HD90722	EW_HD102117
6007,317	28,0	1,68	-3,41	50,8	49,2
6086,288	28,0	4,27	-0,46	70,1	68,1
6108,120	28,0	1,68	-2,43	96,0	93,2
6111,080	28,0	4,09	-0,81	65,7	62,7
6119,760	28,0	4,27	-1,32	23,6	21,9
6130,140	28,0	4,27	-0,94	42,3	39,4
6175,370	28,0	4,09	-0,55	73,7	70,2
6176,798	28,0	4,09	-0,26	89,8	87,2
6177,250	28,0	1,83	-3,51	33,7	32,3
6186,717	28,0	4,11	-0,88	56,2	51,9
6204,605	28,0	4,09	-1,10	43,0	38,2
6223,991	28,0	4,11	-1,05	50,0	45,5
6230,100	28,0	4,11	-1,13	43,1	38,6
6322,169	28,0	4,15	-1,21	37,9	34,7
6327,600	28,0	1,68	-3,06	65,2	62,3
6360,810	28,0	4,17	-1,15	32,9	31,6
6378,258	28,0	4,15	-0,97	56,9	51,9
6482,810	28,0	1,93	-2,76	76,7	73,7
6598,611	28,0	4,24	-0,91	50,0	47,1
6635,130	28,0	4,42	-0,72	46,2	41,6
6643,640	28,0	1,68	-2,03	121,6	119,1
6767,780	28,0	1,83	-2,10	103,5	104,1
6772,320	28,0	3,66	-0,97	77,7	73,7
6842,043	28,0	3,66	-1,50	46,7	43,0
7110,900	28,0	1,94	-2,88	70,7	64,8
7715,591	28,0	3,70	-1,01	74,2	70,2
7748,890	28,0	3,70	-0,38	119,4	116,6
5105,558	29,0	1,39	-1,52	118,6	113,8
5218,202	29,0	3,82	0,48	74,2	74,1
7933,131	29,0	3,79	-0,37	66,4	57,1
6362,347	30,0	5,80	0,14	36,8	34,3
5087,418	39,1	1,08	-0,17	59,9	58,0
5200,411	39,1	0,99	-0,57	55,8	54,7
5853,696	56,1	0,60	-0,91	77,6	77,6
6141,695	56,1	0,70	-0,08	137,0	137,1
6496,900	56,1	0,60	-0,38	115,3	113,4
5274,230	58,1	1,04	0,13	17,2	16,1
6645,100	63,1	1,38	0,12	11,1	9,6